Adverse effects of copper, manganese and mercury, alone and in mixtures on the aorta and heart of Sprague-Dawley rats

M Janse van Rensburg[1], MJ Bester[1], MJ van Rooy[2], HM Oberholzer[1]

[1] Faculty of Health Sciences, Department of Anatomy, University of Pretoria, Arcadia, South Africa

[2] Faculty of Health Sciences, Department of Physiology, University of Pretoria, Arcadia, South Africa

Abstract

Cardiovascular diseases (CVD) are a common global cause of death and is therefore a major health concern. Inhaled or ingested environmental heavy metals contribute to the development of CVD. The aim of this study was to address the limited information available on the effect of relevant dosages of metals in mixtures. Three metals with reported effect on the cardiovascular system (CVS) were identified and these were copper (Cu), manganese (Mn) and mercury (Hg). In Sprague-Dawley rats, the adverse effects of copper (Cu), manganese (Mn) and mercury (Hg), alone and as part of mixtures, on the blood parameters, the aorta and heart was investigated. Forty-eight male Sprague-Dawley rats were randomly divided into eight groups (n=6): control, Cu, Mn, Hg, Cu + Mn, Cu + Hg, Mn + Hg and Cu, Mn + Hg. The seven experimental groups received the metal mixtures at 100 times the World Health Organisation (WHO) safety limit for drinking water (2mg/L for Cu, 0.4mg/L for Mn and 0.06 mg/L for Hg) via oral gavage for 28 days. After 28 days, compared with the control, red blood cell levels were increased for Cu + Hg. All other measured blood parameters were unchanged. Morphological changes in the tunica media were connective tissue deposition and an abundance of collagen type I in the metal exposed aortic tissues. In the cardiac tissue of metal exposed rats, changes in the cardiomyocyte and myofibrillar arrangement, with an increase in collagen type I and III was observed. Ultrastructurally, the aortic collagen and elastin band arrangement and the cardiac mitochondrial and myofibrillar arrangement and structures were altered in the experimental groups. These changes indicate that exposure to these metals in rats causes minor changes in the blood parameters, however the changes in tissue and cellular structure indicates an increased risk for the development of CVD.

Keywords: Cu, Mn, Hg, metal mixtures, aorta, heart, collagen

Introduction

The cardiovascular system (CVS) is vulnerable to damage by environmental pollutants when inhaled or ingested (Cosselman et al., 2015; Kim et al., 2018) and associated pathologies include atherosclerosis, thrombosis, embolism, and infarction. Myocardial infarction and stroke can occur when atherosclerosis is complicated by thrombosis (Kierszenbaum and Tres, 2016). Risk factors associated with CVD development include age, sex, lifestyle, the presence of additional co-morbidities and environmental pollutants including heavy metals (Alissa and Ferns, 2011; Cosselman et al., 2015). These heavy metals occur either naturally or as a result of anthropogenic activity (Mudgal et al., 2010; Jaishankar et al., 2014) and accumulates in the environment including waterways. The World Health Organisation (WHO) has established limits on the levels of heavy metals in drinking water, however due to poor water treatment and the dependence on water from rivers, lakes and dams many communities are increasingly being exposed to heavy metals.

Several factors can impact on the severity of disease as a consequence of exposure, and this includes the dosage and duration of exposure as well as the presence and contribution of other toxic molecules such as heavy metals. A limitation in research on the tissue and cellular effects of heavy metals, is the dosage used in animal studies. Dosages are often based on previous studies, or the levels of a specific metal found in a specific locality. Although these studies are helpful in identifying tissue and cellular targets, the effects of lower relevant dosages are unknown. A further factor is the duration of exposure, whether the model used represents acute or chronic toxicity. Furthermore, environmental exposure is not limited to a single metal, but exposure is usually to a mixture of metals, in which each metal retains its original properties and the concentration of each is variable. If these metals then target a specific aspect of the CVS this can lead to either additive or synergistic effects.

In a previous study Arbi et al., 2021 evaluated the effect of cadmium (Cd) and Hg alone and in combination at the 1000 X WHO limits of each metal on the CVS of Sprague Dawley rats exposed for 28 days. Cd alone caused the most mitochondrial damage while Hg to a greater degree induced fibrosis. In the aorta, both Cd and Hg as a mixture also increased collagen deposition adversely altering the morphology of

the fenestrated elastic fibers in the tunica media. Co-exposure also resulted in increased cardiotoxicity with increased mitochondrial damage, fibrosis and distortion of the aortic wall as a result of increased collagen deposition, as well as altered elastin deposition, fragmentation and interlink formation. These morphological features were the consequence of oxidative damage associated with premature ageing of the CVS that potentially can lead to hypertension and premature cardiac failure.

In this follow-up study the metals, copper (Cu), manganese (Mn) and Hg were selected based on their reported effects on the CVS. Copper causes atherosclerotic plaque formation due to low-density lipoprotein (LDL) oxidation, resulting in CVD such as myocardial infarction (Angelova et al., 2011; Jomova and Valko, 2011). Manganese (Mn) causes myocardial damage due to the inhibition in calcium ion (Ca^{2+}) channels as well as an increase in heart rate and hypotension and vessel permeability associated with CVD (Crossgrove and Zheng, 2004; Hunt, 2007; O'Neal and Zheng, 2014). Mercury exposure is associated with hypertension, coronary heart disease, myocardial infarction, blood vessel obstruction, cardiac arrhythmias, atherosclerosis and endothelial dysfunction (Kumar and Bhattacharya, 2000; Kampa and Castanas, 2008; Lim et al., 2010; Houston, 2011). Furthermore in a previous study (Arbi et al., 2021), Hg was found to induce fibrosis in the CVS. In the present study a 100 X WHO concentrations were selected, to determine the effect of exposure to even lower, and potentially more relevant concentrations of these metals on the CVS.

Therefore, the aim of this study was to investigate the effects of 100 X WHO limit in drinking water of Cu, Mn and Hg alone and in mixtures on the blood, the morphology and ultrastructure of the aorta and heart tissue of Sprague-Dawley (SD) rats following gavage-dosing for 28 days.

Materials and methods

Metal preparation

This study used male SD rats exposed to either saline only (control) or to Cu, Mn and Hg, alone and in mixtures. Administration of the aqueous solutions of copper (II) sulphate ($CuSO_4.5H_2O$, purity: 98%), manganese (II) chloride ($MnCl_2.4H_2O$, purity: 99%), mercuric chloride powder ($HgCl_2$, purity: 99%) and 0.9% sodium chloride (NaCl,

purity: 99%), which were dissolved in distilled, deionised water (ddH_20), occurred via oral gavage. All metal compounds were purchased from Sigma-Aldrich, South Africa.

Dosage calculations

The final daily dosage solutions for the metals are presented in Table 1. The concentrations chosen were based on and were X100 greater than the 2011 WHO drinking water guideline values, for each respective metal (WHO, 2011). The calculated concentrations were based on a 60 kg adult drinking 2 L of water a day. A 150 g rat equivalent dosage was then calculated, using the following equation:

Rat equivalent dose (mg/kg) = Human equivalent dose (mg/kg) / dosage factor*

*Dosage factor being rat Km/human Km, with the human Km = 37 and the rat Km = 6.

Table 1: Dosage calculations for the oral gavage solutions of the experimental groups.

	Cu	Mn	Hg
WHO limit (mg/L)	**2.0**	**0.4**	**0.006**
WHO limit X 100 (mg/L)	200.0	40.0	0.6
Molecular weight: metal (g/mol)	63.5	54.9	200.6
Metal ion concentration (mM)	3.147	0.728	0.003
Molecular weight: metal-salt (g/mol)	249.7	197.9	271.5
Metal salt concentration (g/L)	0.786	0.144	0,0008
Daily intake (g/2L)	1.572	0.288	0.0016
Human (60 kg) daily intake (mg/kg)	26.2	4.8	0.027
Rat (150 g) intake (mg/kg)	161.5	29.6	0.17
Dosage solutions (mg/mL)	**48.5**	**8.9**	**0.05**

*Note: Mixtures require the same (mg) of each respective metal.

The dosage factor for conversion from rat to human is 6/37. Km is a correction factor used based off the surface area of a species (Nair and Jacob, 2016). Therefore, the rat equivalent dose is 161.5, 29.6 and 0.17 mg/kg/day for Cu, Mn and Hg, respectively.

Sprague-Dawley rat model

Six-week-old male SD rats (150 g) were obtained from the Onderstepoort Veterinary Animal Research Unit (OVARU). Standard irradiated “Epol” rat pellets and municipal water were provided *ad libitum.* The animals were housed in conventional cages complying with the sizes described in the South African National Standards (SANS)

10386:2008 recommendations. A room temperature of 22°C (±2°C); relative humidity of 50% (±20%) and a 12-hour light/dark cycle was maintained during the entire study. The rats were housed in pairs in cages with autoclaved pinewood shavings as bedding material. White facial tissue paper was added for enrichment according to standard procedures at the UPBRC. The rats were acclimatized for 7 days prior to the start of the 28-day experimentation period. Ethical approval was obtained from the University of Pretoria's Animal Ethics Committee (AEC) with approval number 6/2019.

Forty-eight male rats were included and were randomly divided into eight groups (six rats per group), as follows: control, Cu, Mn, Hg, Cu + Mn, Cu + Hg, Mn + Hg and Cu, Mn + Hg (The control group received a saline solution, 0.9% NaCl, only). The seven experimental groups received the metal mixtures assigned, at a X100 the World Health Organisation (WHO) safety limit for drinking water (2mg/L for Cu, 0.4mg/L for Mn and 0.06 mg/L for Hg) (WHO, 2011). A rat equivalent dosage was then calculated (Nair and Jacob, 2016). All rats were administered 0.5 mL of the respective solutions daily through oral gavage, for 28 days. The rats were weighed bi-weekly to identify any sudden change in weight and the behaviour of the rats was monitored daily. The rats were terminated on day 28 via isoflurane (general anaesthesia) overdose and cardiac puncture, according to the standard methods employed by the UPBRC.

Blood collection and analysis

Blood was collected on the day of termination via cardiac puncture into 4.5 mL EVAC EDTA tubes and sent to Ampath and to the Onderstepoort Clinical Pathology Department, University of Pretoria for the determination of the level of the metals in circulation and for a full blood count (FBC) analysis, respectively. The levels of Cu, Mn and Hg in the blood were quantified with inductively coupled plasma mass spectrometry (ICP-MS) – Table 2. The results of the FBC investigated to evaluate the toxicity of the metals are shown in Table 3. Several blood parameters were measured and included haemoglobin (Hb) levels, the haematocrit (HCT), the mean corpuscular volume (MCV), the mean corpuscular haemoglobin (MCH), the mean corpuscular haemoglobin concentration (MCHC), the white cell count (WCC), segmented neutrophils (SNEU), lymphocytes (LYM), monocytes (MON), eosinophils (EOS) and basophils (BAS) were determined.

Organ harvesting

Organs were harvested on the day of termination after blood collection via dissection. The upper thoracic portion of the descending aorta and the myocardium of the apex (left ventricle) of the heart for all the rats were harvested and prepared for light- and transmission electron microscopy.

Light microscopy sample preparation

All reagents were obtained from Sigma Aldrich, Johannesburg, South Africa unless otherwise specified. The aorta and heart were dissected from each animal at the time of termination and processed for light microscopy. The tissue samples were fixed overnight in 4% formaldehyde (FA) in 0.1 M phosphate buffer solution (PBS) [0.2 M disodium phosphate (Na_2HPO_4), 0.2 M sodium dihydrogen phosphate monohydrate ($NaH_2PO_4 \cdot H_2O$), 0.15 M sodium chloride (NaCl), pH: 7.4]. The fixed tissues were sent to the Department of Paraclinical Sciences in the section of Pathology at the faculty of Veterinary Sciences of the University of Pretoria for the preparation of paraffin blocks and unstained slides as follows: After overnight fixation, the samples were washed three times for 30 minutes with 0.1 M PBS and then dehydrated using increasing serial concentrations of ethanol (EtOH) (50%, 70%, 90% and 100%). Dehydration occurred in the following sequence: 50% EtOH for 30 minutes, 70% EtOH for one hour, 90% EtOH for one hour, twice in 100% EtOH for one hour and left overnight in 100% EtOH. The samples were infiltrated with paraffin wax by first placing them in a 1:1 xylene and ethanol mixture for 30 minutes, then 100% xylene for 2 hours, followed by 3:7 wax in xylene mixture for one hour, 7:3 wax in xylene mixture for one hour and finally in 100% wax for two hours. All steps involving wax infiltration were undertaken at 60˚C. The samples were embedded in paraffin wax and then cooled to 4˚C prior to sectioning. The prepared blocks were sectioned at a thickness of 5 µm using a microtome (Leica RM2255) and placed on glass slides. For de-waxing, the slides were placed twice in 100% xylene for five minutes, and then twice in 100% ethanol for two minutes. The slides were then rehydrated in 90% and 70% ethanol for one minute each and finally in deionised and distilled water (ddH_2O) for 1 minute.

Haematoxylin and eosin staining

For general structural studies of aorta and heart tissue, haematoxylin and eosin (H&E) staining was performed to identify nuclei and cell morphology. This was done by the Department of Paraclinical Sciences in the section of Pathology at the faculty of Veterinary Sciences of the University of Pretoria by following standard laboratory protocol. The slides were viewed with a Zeiss AXIO Imager.M2 (Carl Zeiss Microscopy, Munich, Germany) light microscope.

Picrosirius red staining

The Picrosirus red (PR) staining and polarisation method is a simple technique that is specific and sensitive to collagen staining. It is used to determine the orientation of collagen fibres in different tissues under different pathological and physiological states (Latouff et al., 2014). Collagen appears red, green or yellow under polarized light. A strong yellow-red birefringence indicates collagen type I and a weak greenish birefringence indicates collagen type III (Latouff et al., 2014). A mass of 0.5 g of Sirius Red dye was dissolved in 500 mL of a saturated aqueous solution of picric acid. Acidified water was used for washing, prepared by adding 5 mL of glacial acetic acid to 1 L of ddH_2O. The tissue was first stained in haematoxylin for eight minutes and then rinsed under running tap water for ten minutes. The PR solution was applied for 1 hr and the slides were washed twice with acidified water. The tissue was dehydrated three times in 100% EtOH and cleared with xylene before the coverslip was mounted using Entellan (Velindala et al., 2014). The slides were viewed with a Zeiss AXIO Imager.M2 (Carl Zeiss Microscopy, Munich, Germany) light microscope, under brightfield and polarizing light.

Transmission electron microscopy sample preparation

For ultrastructural studies of aorta and heart, TEM was performed. Samples were obtained from the same area as for light microscopy. The tissue samples were cut into small pieces of approximately 1 mm^3 in size. The tissue samples were then fixed in a 2.5% glutaraldehyde/formaldehyde (GA/FA) (Sigma-Aldrich, South Africa (SA)) (5 mL 0.075 M phosphate buffered saline (PBS) – pH 7.4), 1 mL GA, 1 mL FA and 3 mL deionised distilled water (ddH_20) – solution for one hr before being washed three times in the same buffer for 15 minutes each time. The samples then underwent secondary

fixation in 1% osmium tetroxide (Sigma-Aldrich, SA) for one hr and were washed again as described in the previous step. The samples were dehydrated by using an increasing serial dehydration step with 30%, 50%, 70% and 90%, followed by three changes of 100% ethanol (EtOH) for 15 minutes each step. The samples were then left in 100% EtOH (Merck, SA) overnight. Following the overnight dehydration, the samples were embedded in resin (Arbi et al., 2021).

The resin samples were trimmed and ultra-thin sections (100 nm) were made using an ultramicrotome. Samples were contrasted with uranyl acetate for three minutes followed by three minutes of contrasting with lead citrate, after which samples were allowed to air dry before being examined with the JEOL JEM 2100F transmission electron microscope (JEOL Ltd., Tokyo, Japan). Representative images of each group were used to evaluate the changes in tissue ultrastructure.

Statistical analysis

Statistical analysis on the levels of the heavy metals in the blood, the FBC, the biochemical parameters and the weight differences were performed on GraphPad Prism version 6.01, using one-way analysis of variance (ANOVA) and Tukey's multiple comparisons test. A p-value of < 0.05 was considered significant.

Tissue evaluation

This observational qualitative study of eight animal groups, consisting of the control and seven heavy metal exposed groups, aimed to describe the general structure (H&E staining) and fibrosis (PR staining) in the heart and aortic tissue using LM and the ultrastructure using TEM. The changes in tissue structure in the exposed groups were compared with the control group. Six rats were included in each group and for each staining method two slides from each rat were analysed with LM and for each of the tissues two grids for each animal were analysed with TEM. The most representative findings are presented in Figure 1-10.

For comparative purposes a scoring system was used, where the degree of change was evaluated. The parameters that were evaluated using LM in aorta were the extent of nuclear shape changes, the appearance of increased thickness of the tunica media layer, uneven thickness of the aorta wall, presence of foam cells, increase in

perinuclear spaces and an increase in connective tissues. In cardiac tissue the parameters evaluated were the extent of tissue arrangement/dilatation, nuclear changes, myofibrillar destruction, lipid droplet accumulation, lymphocyte infiltration and extracellular matrix (ECM) deposition.

The parameters that were evaluated using TEM in aorta were the extent of band disarrangement, collagen deposition, and elastin disruption, changes in electron density, elastin fragmentation and lipid accumulation. In cardiac tissue the parameters evaluated were the extent of myofibrillar disorganization, mitochondrial cristae swelling, myofibrillar Z line alterations, vacuolation and necrosis. For all the parameters the scoring was –: no or minimal alterations; +: slight alteration; ++: moderate alteration and +++: severe alteration based on the degree of change of the tissues.

Results

Plasma levels of the heavy metals

The blood levels of each metal on the day of termination were determined (Table 2). Copper levels were increased for all groups, compared with the control, but was only statistically significantly increased in the Cu + Mn group. The Mn levels were increased in all groups, compared with the control, with Mn + Hg and the triple mixture group showing a significant increase. For Hg a statistical significant increase in levels was observed for Hg and Mn + Hg, as compared with the control.

Table 2: Plasma levels (mean ± standard deviation) of Cu, Mn and Hg in exposed rats on day 28.

Group	Cu (µg/L)	Mn (µg/L)	Hg (µg/L)
Control	558 ± 68	4.7 ± 0.7	BDL (<1.0)
Cu	670 ± 56	-	-
Mn	-	6.0 ± 0.6	-
Hg	-	-	2.3 ± 1.3*
Cu + Mn	738 ± 77*	5.6 ± 1.0	-
Cu+ Hg	672 ± 79	-	BDL (<1.0)
Mn + Hg	-	6.3 ± 0.5*	5.6 ± 1.0*
Cu, Mn + Hg	660 ± 69	6.5 ± 1.0*	BDL (<1.0)

*Significant compared with control levels of each metal.

Table 3: The FBC parameters (mean ± standard deviation) of control and exposed rats measured on day 28.

Red blood cell parameters								
Metal mixtures	**None**	**Single**			**Double**			**Triple**
	Control	**Cu**	**Mn**	**Hg**	**Cu + Mn**	**Cu + Hg**	**Mn + Hg**	**Cu, Mn + Hg**
Hb (g/L)	166 ± 4.5	161 ± 4.4	157 ± 1.8	159 ± 8.8	164 ± 6.5	157 ± 6.5	164 ± 6.2	163 ± 7.3
RBC (X 10^{12}/L)	9.3 ± 0.3	9.0 ± 0.3	9.0 ± 0.6	8.8 ± 0.5	9.2 ± 0.5	9.3 ± 0.6[1]	8.8 ± 0.4	9.3 ± 0.4
HCT(%)	51 ± 1.0	49 ± 1.0	48 ± 1.0	48 ± 3.0	50 ± 2.0	49 ± 2.0	49 ± 2.0	50 ± 3.0
MCV (fL)	54.7 ± 1.7	54.6 ± 1.5	53.8 ± 3.1	55.3 ± 2.3	54.6 ± 1.6	52.8 ± 4.3	55.0 ± 0.6	54.5 ± 0.6
MCH (pg)	18.2 ± 0.8	18.0 ± 0.5	17.6 ± 1.2	18.0 ± 1.0	17.9 ± 0.8	17.1 ± 1.7	18.5 ± 0.3	17.5 ± 0.3
MCHC (g/L)	332 ± 5.0	330 ± 4.0	326 ± 3.0	333 ± 6.0	327 ± 6.0	323 ± 7[3]	337 ± 4[2]	322 ± 5[3,6]
RDW (%)	10.9 ± 0.3	11.7 ± 0.6	10.9 ± 0.5	10.9 ± 0.5	11.4 ± 0.4	12.1 ± 0.	11.1 ± 0.2	11.5 ± 0.7
White blood cell parameters								
	None	**Single**			**Double**			**Triple**
Metal mixtures	**Control**	**Cu**	**Mn**	**Hg**	**Cu + Mn**	**Cu + Hg**	**Mn + Hg**	**Cu, Mn + Hg**
WCC (X 10^9/L)	11.0 ± 1.9	11.7 ± 2.3	12.1 ± 2.0	9.4 ± 3.4	13.9 ± 3.3	12.0 ± 1.8	10.7 ± 2.1	11.4 ± 1.6
SNEU (X 10^9/L)	1.7 ± 0.4	2.2 ± 1.2	1.7 ± 0.7	1.3 ± 0.6	3.5 ± 3.5	1.9 ± 0.1	2.3 ± 0.9	1.7 ± 0.3
LYM (X 10^9/L)	9.0 ± 1.6	28.3 ± 42.9	9.9 ± 1.8	7.7 ± 2.8	9.7 ± 1.40	9.3 ± 1.5	7.8 ± 1.6	25.1 ± 36.4
MON (X 10^9/L)	0.24 ± 0.22	0.22 ± 0.13	0.45 + 0.4	0.32 ± 0.4	0.48 ± 0.28	0.34 ± 0.16	0.33 ± 0.04	0.33 ± 0.12
EOS (X 10^9/L)	0.06 ± 0.06	0.03 ± 0.06	0.07 ± 0.1	0.05 ± 0.05	0.19 ± 0.20	0.30 ± 0.37	0.23 ± 0.13	0.09 ± 0.05
BAS (X 10^9/L)	0.02 ± 0.05	0.00 ± 0.00	0.00 ± 0.0	0.01 ± 0.02	0.02 ± 0.04	0.03 ± 0.06	0.02 ± 0.04	0.01 ± 0.03
Platelets								
Metal mixtures	**None**	**Single**			**Double**			**Triple**
	Control	**Cu**	**Mn**	**Hg**	**Cu + Mn**	**Cu + Hg**	**Mn + Hg**	**Cu, Mn + Hg**
PLT (X 10^9/L)	639 ± 151	648 ± 231	542 ± 168	611 ± 128	644 ± 183	687 ± 161	751 ± 40	820 ± 161

Statistical difference vs control (*), vs Cu ([1]), Mn ([2]) or Hg([3]), vs Cu + Mn ([4]), Cu + Hg ([5]), Mn + Hg ([6]) or the triple mixture.

Full blood count analysis

The FBC parameters of the control and experimental groups were determined (Table 3) using the blood taken on the day of termination. The Hb, RBC, HCT, MVC and MCH were unchanged. Compared with the control the RBC number was only increased for Cu + Hg. For the MCHC levels for all exposure groups were unchanged compared with the control. Levels were reduced for Hg vs Cu + Hg, Mn vs Mn + Hg, Hg vs Cu, Mn + Hg and Mn + Hg vs Cu, Mn + Hg. All other measured blood parameters were unchanged.

Aorta

Light microscopy

The general histology of the aortic layers (tunica intima, media and adventitia) and the arrangement of the endothelial cells, smooth muscle cells and connective tissue were evaluated using H&E staining. Representative images, at X40 magnification, acquired from stained aorta tissue are shown in Figure 1. In Figure 1A, the aorta of the control (saline) group is shown with the tunica intima (TI), tunica media (TM) and tunica adventitia (TA). The aortic walls have an even thickness throughout, with the smooth muscle cell nuclei (SMCN) oval in shape. In the aortic tissue from the control (saline) group some perinuclear spaces (black ring) are present. The aortic tissues of the experimental groups are shown in Figures 1B - H. The layers of the aorta have an uneven thickness in all the experimental groups. The tunica media appears thicker in the Cu, Mn and Cu + Mn groups (B, C and F). Flattened SMCN (red arrows) and the appearance of foam cells (orange arrows) were observed in all experimental groups except for Cu + Mn (B, C, D, E, G and H). Small and round SMCN (blue arrows) were observed in all mixtures (E, F, G and H). The appearance of more prominent perinuclear spaces (black ring) was observed in Cu, Mn, Hg and Mn + Hg (B, C, D and G). The connective tissue layer (red ring) between the SMCs appeared thicker in the Mn, Hg, Cu + Mn and triple mixture groups (C, D, E and H). The Cu and Mn groups showed the most prominent structural changes to aortic architecture, when compared with the other groups.

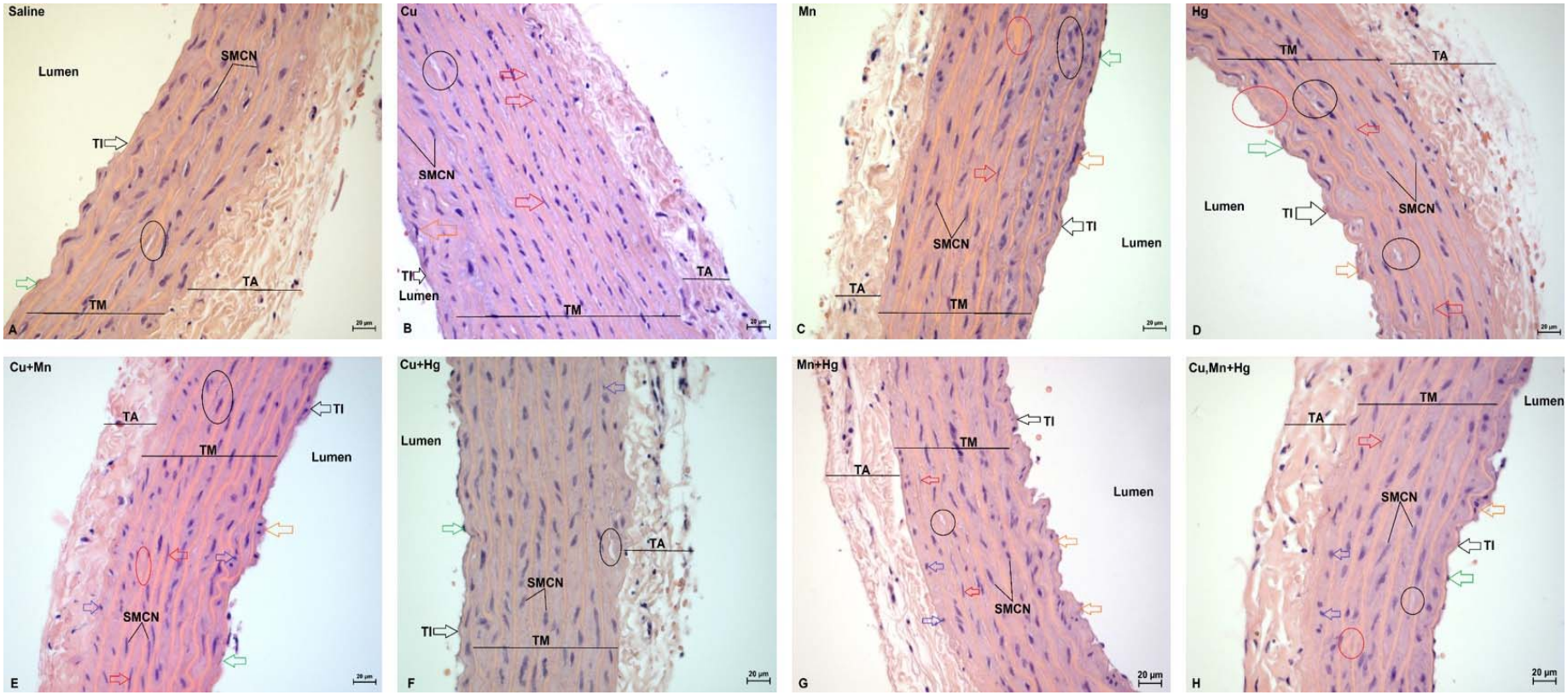

Figure 1: Photomicrographs of SD rat aorta stained with H&E; Scale bar = 20 µm. **A**: Control, **B**: Cu, **C**: Mn, **D**: Hg, **E**: Cu + Mn, **F**: Cu + Hg, **G**: Mn + Hg, and **H**: Cu, Mn + Hg. **TI**: Tunica intima; **TM**: Tunica media; **TA**: Tunica adventitia; **SMCN**: smooth muscle cell nuclei; **Green arrow**: Endothelial cell; **Red arrow**: Flattened nuclei; **Orange arrow**: Foam cell; **Blue arrow**: Small, round nuclei; **Red ring**: Prominent connective tissue and **Black ring**: Prominent perinuclear space.

A summary on the morphological findings of the aortas is presented in Table 4 with the severity of the changes indicated.

Table 4: Summary of the histological changes to the H&E stained aorta following metal exposure.

	Flattened/round SMCN	Thicker TM	Uneven thickness	Foam cells	Increase in perinuclear spaces	Increase in connective tissue
Cu	+	+++	+	+	+	-
Mn	+	+	+	++	+	+++
Hg	+	-	+	+	++	+
Cu + Mn	++	-	+	++	-	+
Cu + Hg	+	+	+	-	-	-
Mn + Hg	++	-	+	++	+	-
Cu, Mn + Hg	+	-	+	+	-	+

–: no or minimal alterations; +: slight alteration; ++: moderate alteration; +++: severe alteration

Polarised light microscopy

Collagen differentiation and distribution in the aorta were evaluated with PR staining. Representative images, at X40 magnification, acquired from stained aortic tissue are shown in Figures 2 and 3. In Figure 2 A2, aortic tissue of the control (saline) group is depicted and demonstrates a predominantly green birefringence under polarized light, in the tunica adventitia. The aortic tissues of the experimental groups are presented in Figures 2B – D and 3E – H. An increase in yellow-red birefringence was evident in Cu, Mn, Cu + Mn and Mn + Hg groups (Figures 2 B2 and C2; Figures 3 E2 and G2). The Cu (Figure 2 B2) group had a slight increase, with Mn (Figure 2 C2) having a moderate increase and Cu + Mn (Figure 3 E2) and Mn + Hg (Figure 3 G2) having a severe increase. Interestingly the triple mixture group did not show an increase in this yellow-red birefringence, whereas all other groups containing Mn did.

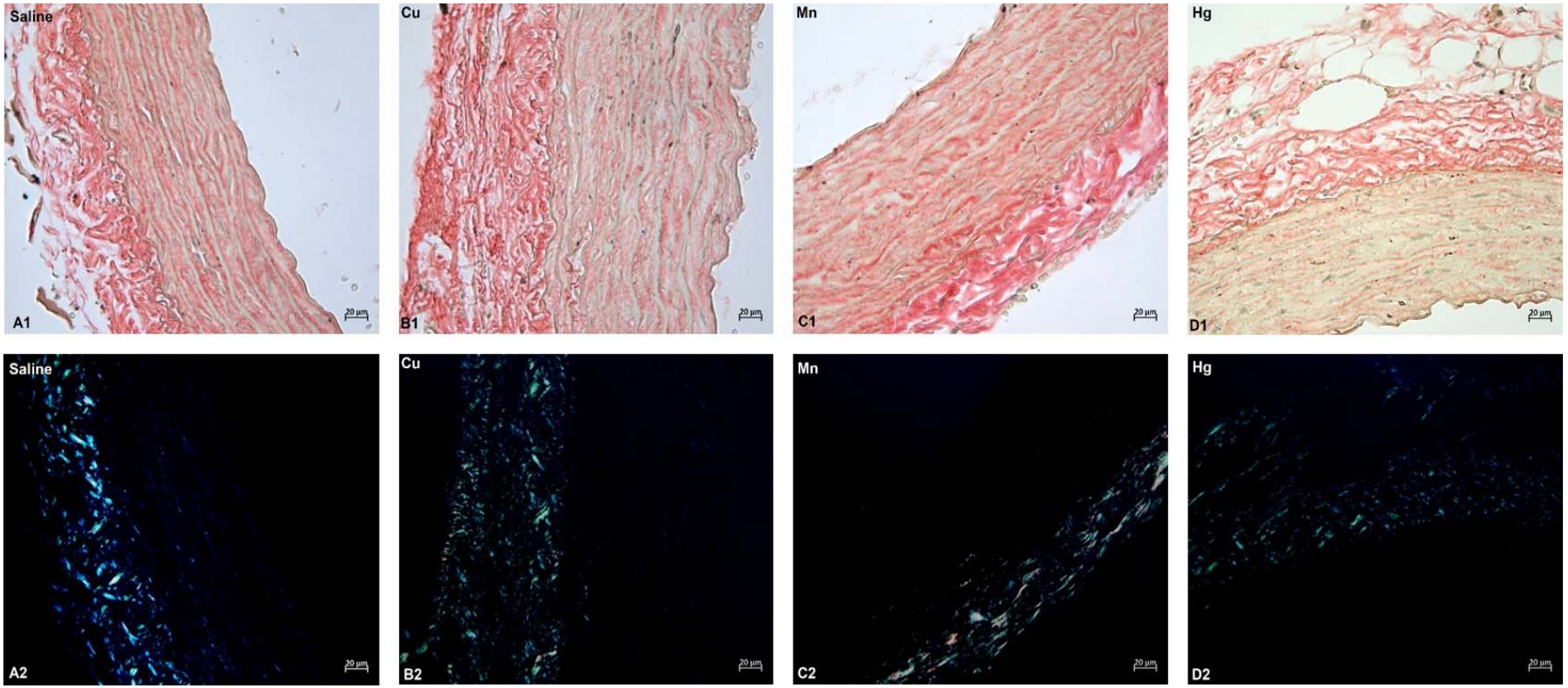

Figure 2: Photomicrographs of SD rat aorta stained with PR for the control and single heavy metal groups; Scale bar = 20 µm. **A**: Control, **B**: Cu, **C**: Mn, **D**: Hg. **1**: Brightfield and **2**: Polarized light.

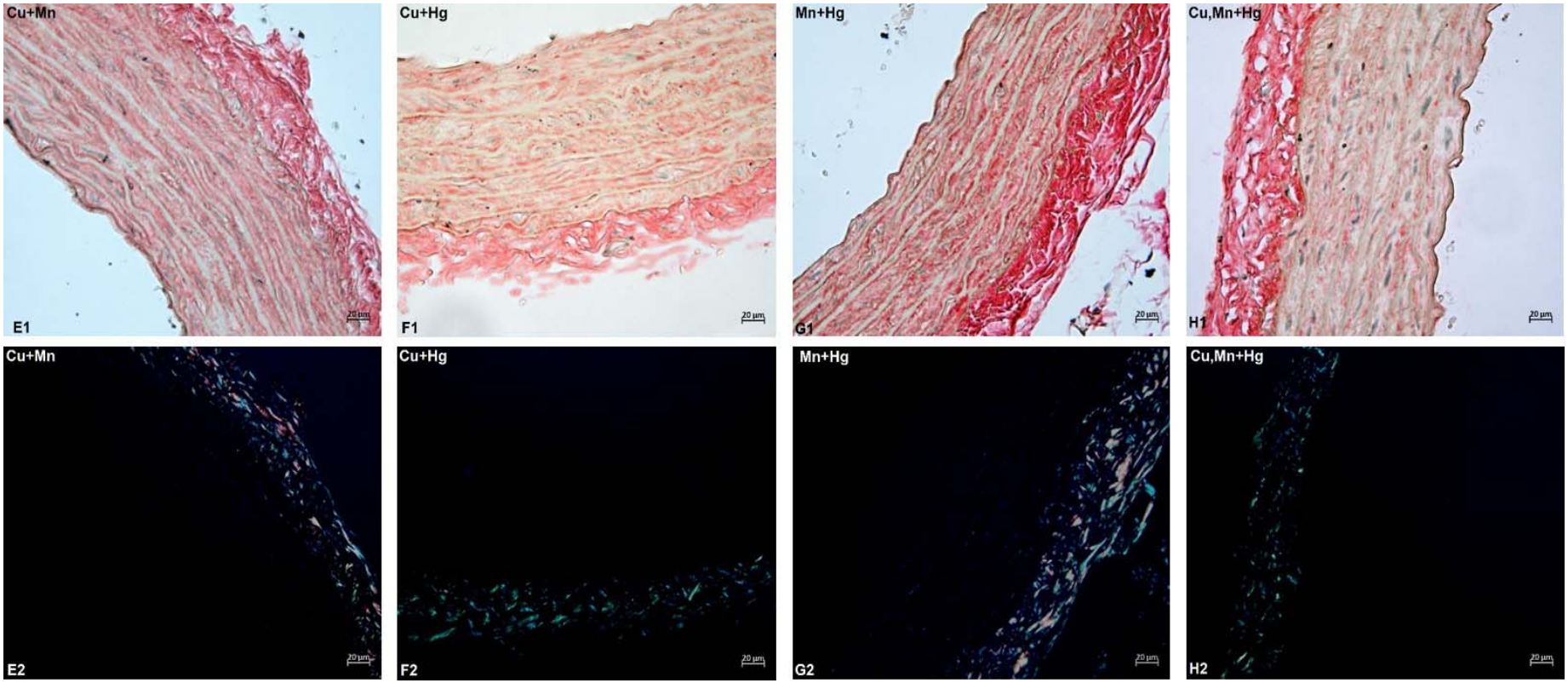

Figure 3: Photomicrographs of SD rat aorta stained with PR for the double and triple heavy metal mixture groups; Scale bar = 20 µm. **E**: Cu + Mn, **F**: Cu + Hg, **G**: Mn + Hg, and **H**: Cu, Mn + Hg. **1**: Brightfield and **2**: Polarized light.

Heart

Light microscopy

The general histology of cardiac tissue was evaluated with H&E staining. Representative images, at X40 magnification, acquired from the stained myocardium are shown in Figure 4. In Figure 4A, heart tissue of the control (saline) group is depicted with typical oval, centred nuclei of the cardiomyocytes (CMN) and branching, striated myofibrils that are continuous and parallel to each other. Blood vessels (black arrows) and erythrocytes (Er) are also indicated and can often be visible throughout the myocardial sections. The myocardium showed a regular, organised arrangement of myofibrils in the tissue from the control (saline) group. The cardiac tissues of the experimental groups are presented in Figures 4B – H. The histological architecture of the myocardium showed cardiomyocyte disarray (loss of normal parallel alignment) in all the experimental groups. Irregular CMN shape, including flattened nuclei (orange arrows) was observed in all experimental groups except for Cu (C to H). Loose myofibrillar arrangement and tissue dilation (asterisk), destruction of myofibrils (red arrows) and the deposition of ECM (blue arrows) were demonstrated in all the experimental groups (B to H) at varying degrees. The accumulation of lipid droplets within the tissue (green arrows) was observed in the Cu, Mn, Hg, Cu + Mn and the triple mixture groups (B, C, D, F and H). Lymphocyte infiltration (black ring and rectangle) was observed in the Cu + Mn, Cu + Hg and the triple mixture group (E, F and H). The Cu + Hg group demonstrated the most structural changes to myocardium architecture, when compared with all other groups.

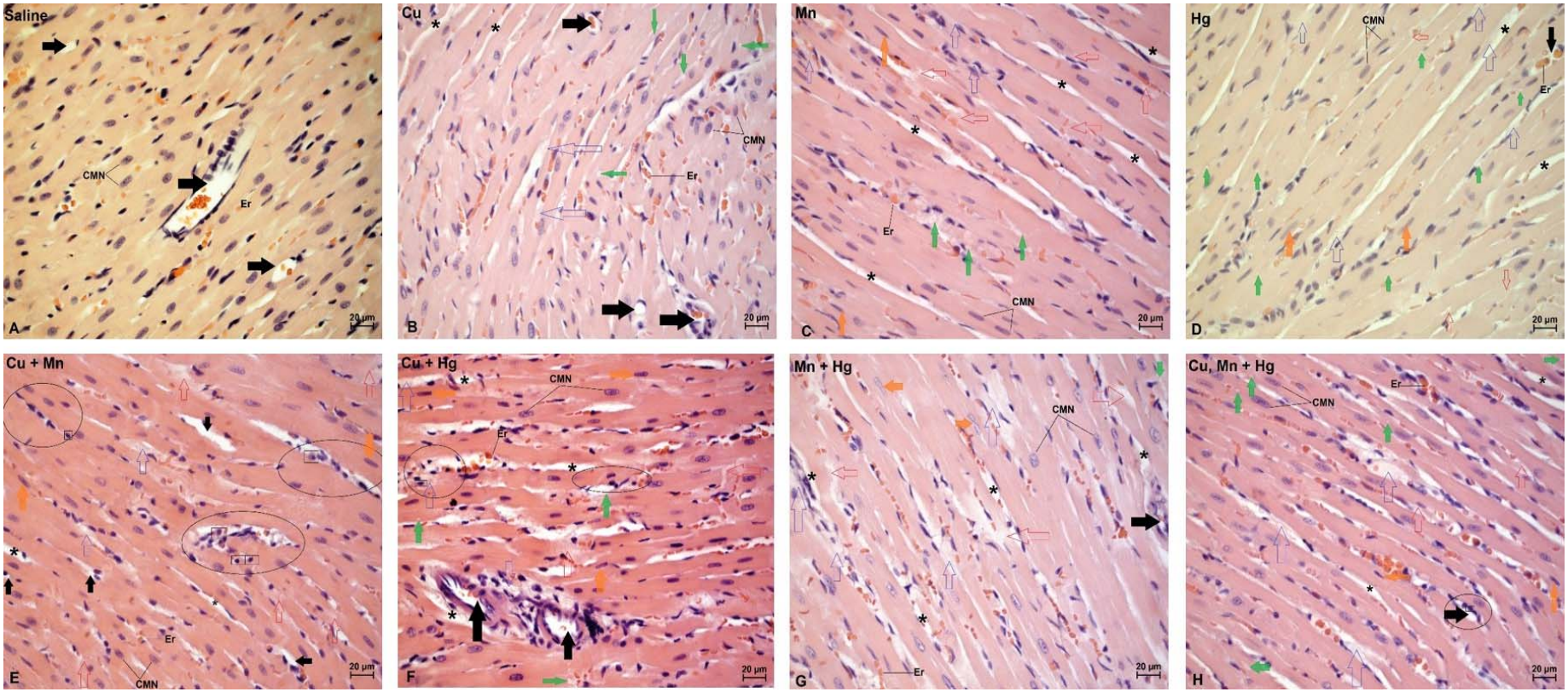

Figure 4: Photomicrographs of SD rat heart tissues stained with H&E; Scale bar = 20 µm. **A**: Control, **B**: Cu, **C**: Mn, **D**: Hg, **E**: Cu + Mn, **F**: Cu + Hg, **G**: Mn + Hg, and **H**: Cu, Mn + Hg. **Er**: erythrocytes; **CMN**: cardiomyocyte nuclei; **Black arrow:** blood vessel or capillary; **Red arrow**: myofibril destruction; **Orange arrow**: Flattened nuclei; **Blue arrow**: ECM deposition; **Green arrow**: Lipid droplet; **Black ring**: Site of lymphocyte infiltration; **Black rectangle**: individual lymphocyte; and **Asterisk (*)**: Tissue dilation.

A summary on the morphological findings of the heart tissue is presented in Table 5 with the severity of the changes indicated.

Table 5: Summary of the histological changes to the H&E stained heart following metal exposure.

	Loose myofibrillar arrangement/ Tissue dilation	CMN changes (including flattened nuclei)	Myofibril destruction	Lipid droplets within tissue	Lymphocyte infiltration	ECM deposition
Cu	+	-	+	+	-	+
Mn	+	+	++	++	-	++
Hg	+	+	+	+	-	+
Cu + Mn	+	++	+++	-	++	++
Cu + Hg	++	++	+++	+	+	++
Mn + Hg	+	++	++	-	-	+
Cu, Mn + Hg	++	++	++	+	+	+

–: no or minimal alterations; +: slight alteration; ++: moderate alteration; +++: severe alteration

Polarised light microscopy

Collagen differentiation and distribution in the cardiac tissues were evaluated using PR staining. Representative images, at X40 magnification, acquired from stained cardiac tissue are shown in Figures 5 to 8. In Figure 5 A2, cardiac tissue of the control (saline) group is depicted and shows a predominantly green birefringence under polarized light, indicative of collagen that surrounds the blood vessel (Figure 5) and is present in the myocardium (Figure 7). The cardiac tissue of the experimental groups are shown in Figures 5 B – D and 6 E – H as well as Figures 7 B – D and 8 E – H. In Figures 5 and 6, an increase in yellow-red birefringence was evident in the Cu, Mn, Mn + Hg and the triple mixture groups (5 B2 and C2 and 6 F2, G2 and H2). The Cu (Figure 5 B2) group had a moderate increase, with Mn (Figure 5 C2), Mn + Hg (Figure 6 G2) and the triple mixture (Figure 6 H2) groups indicating a slight increase and Cu + Hg (Figure 6 F2) a significant increase. However, Mn + Hg and the triple mixture group had a moderate and dramatic increase in yellow-green birefringence, respectively. In Figures 7 and 8, an increase in yellow-red birefringence was observed in Cu and Cu + Hg (Figure 7 B2 and Figure 8 F2). Yellow-green birefringence was extensively present in the triple mixture group (Figure 8 H2), moderately in Hg (Figure 7 D2) and Mn + Hg (Figure 8 G2) and slightly in Cu (Figure 7 B2) and Mn (Figure 7 C2).

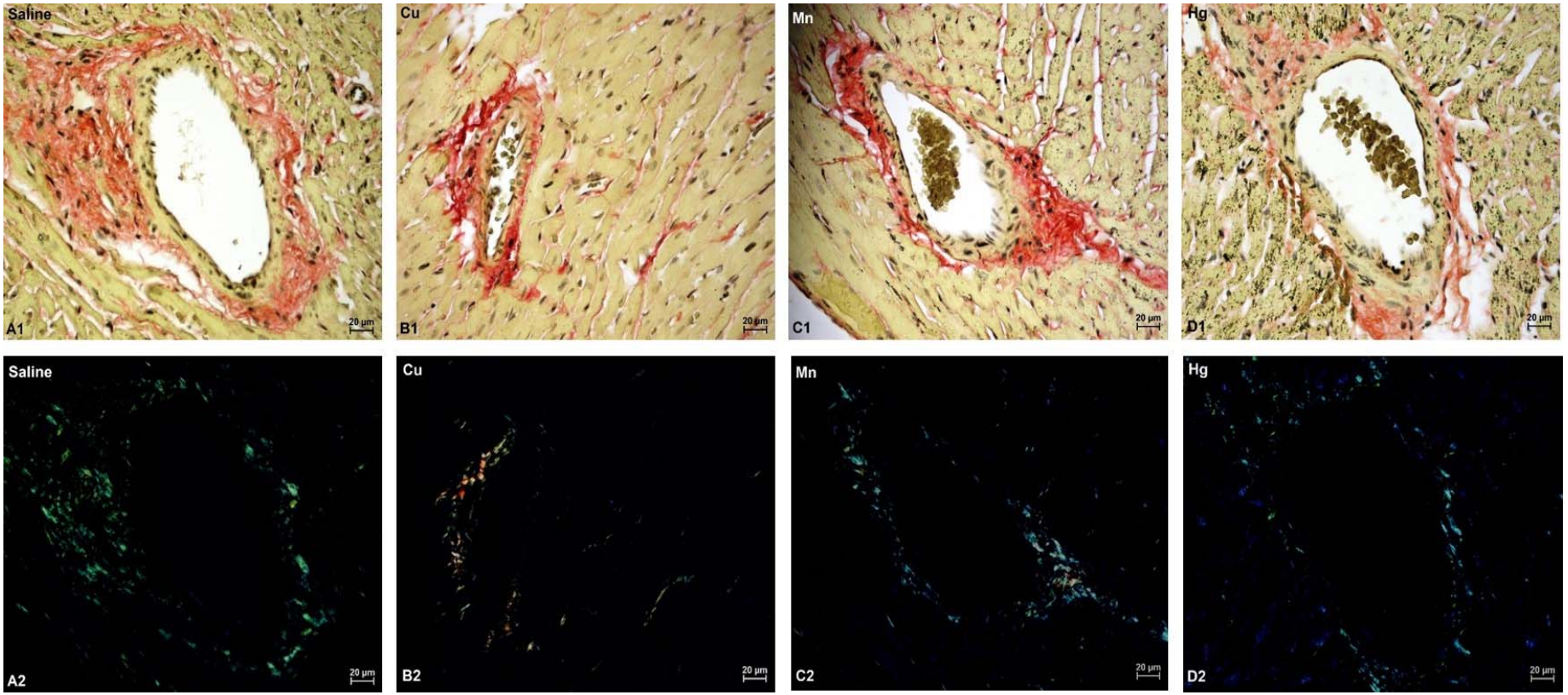

Figure 5: Photomicrographs of SD rat heart stained with PR for the control and single heavy metal groups demonstrating collagen surrounding blood vessels; Scale bar = 20 µm. **A**: Control, **B**: Cu, **C**: Mn, **D**: Hg. **1**: Brightfield and **2**: Polarized light.

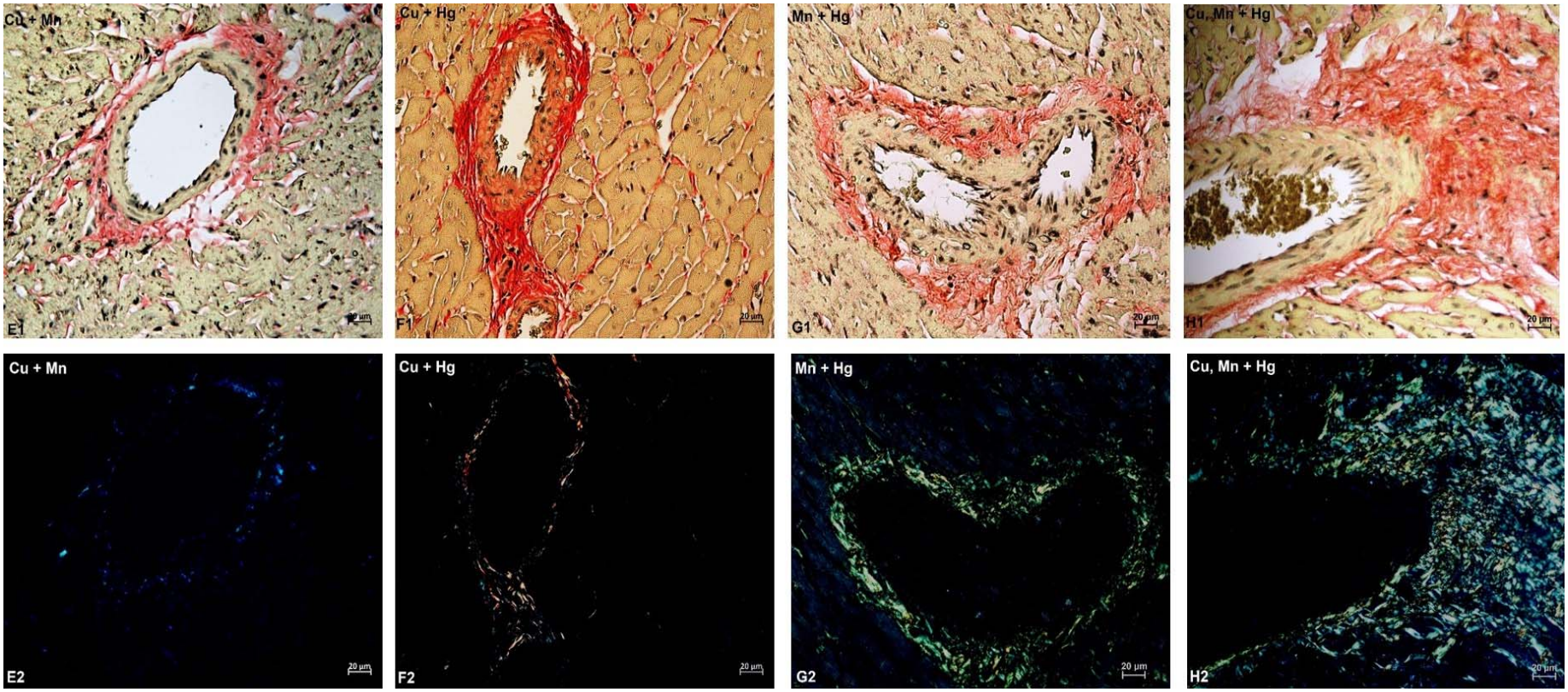

Figure 6: Photomicrographs of SD rat heart stained with PR for the double and triple heavy metal mixture groups demonstrating collagen surrounding blood vessels; Scale bar = 20 µm. **E**: Cu + Mn, **F**: Cu + Hg, **G**: Mn + Hg, and **H**: Cu, Mn + Hg. **1**: Brightfield and **2**: Polarized light.

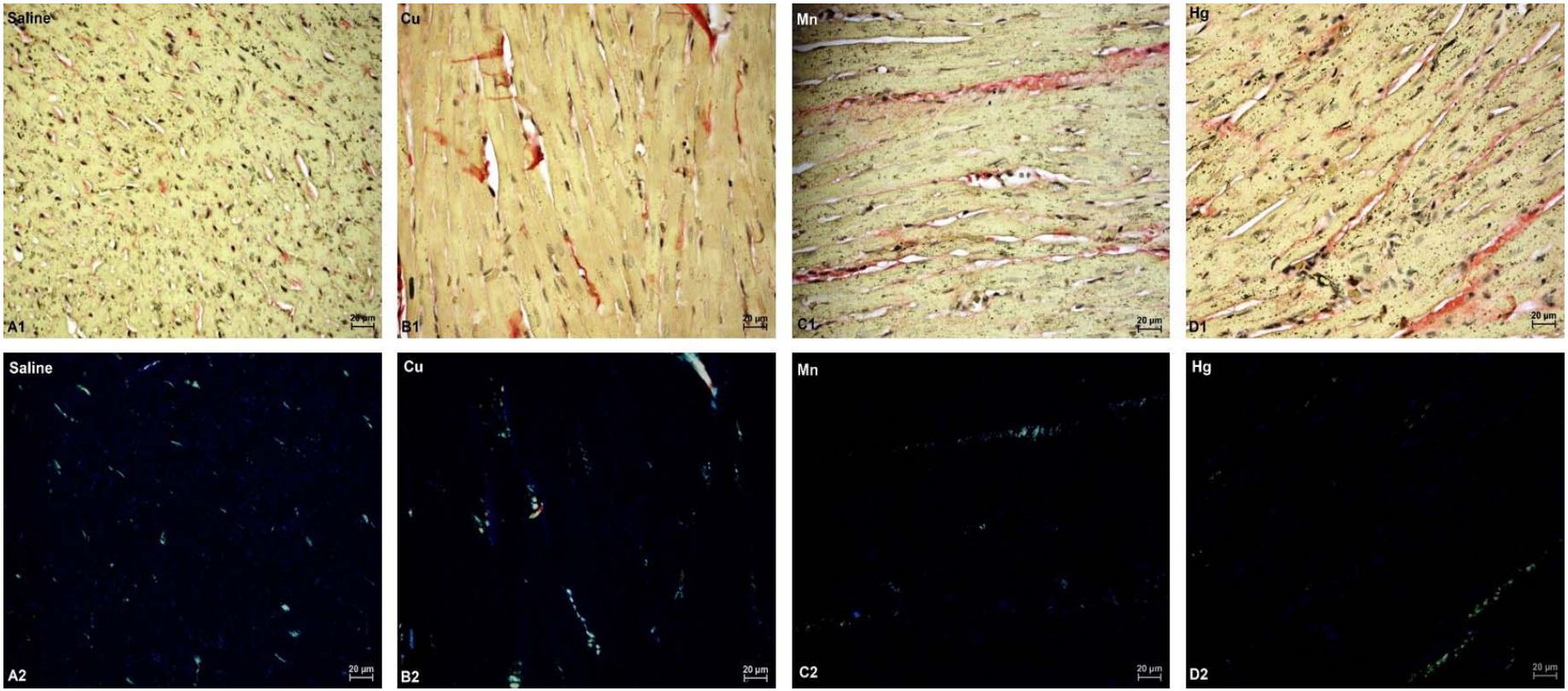

Figure 7: Photomicrographs of SD rat heart stained with PR for the control and single heavy metal groups demonstrating collagen in the myocardium; Scale bar = 20 µm. **A**: Control, **B**: Cu, **C**: Mn, **D**: Hg. **1**: Brightfield and **2**: Polarized light

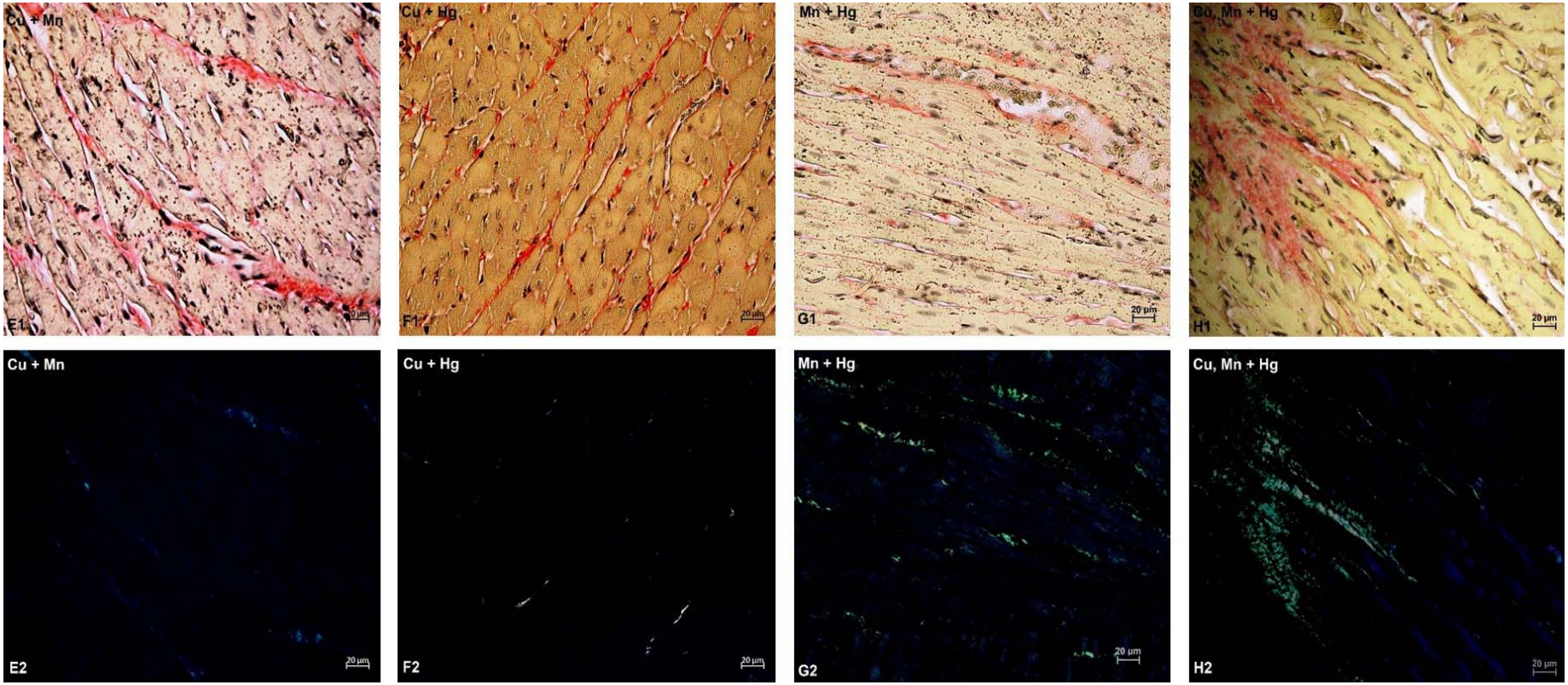

Figure 8: Photomicrographs of SD rat heart stained with PR for the double and triple heavy metal mixture groups demonstrating collagen in the myocardium; Scale bar = 20 µm. . **E**: Cu + Mn, **F**: Cu + Hg, **G**: Mn + Hg, and **H**: Cu, Mn + Hg. **1**: Brightfield and **2**: Polarized light

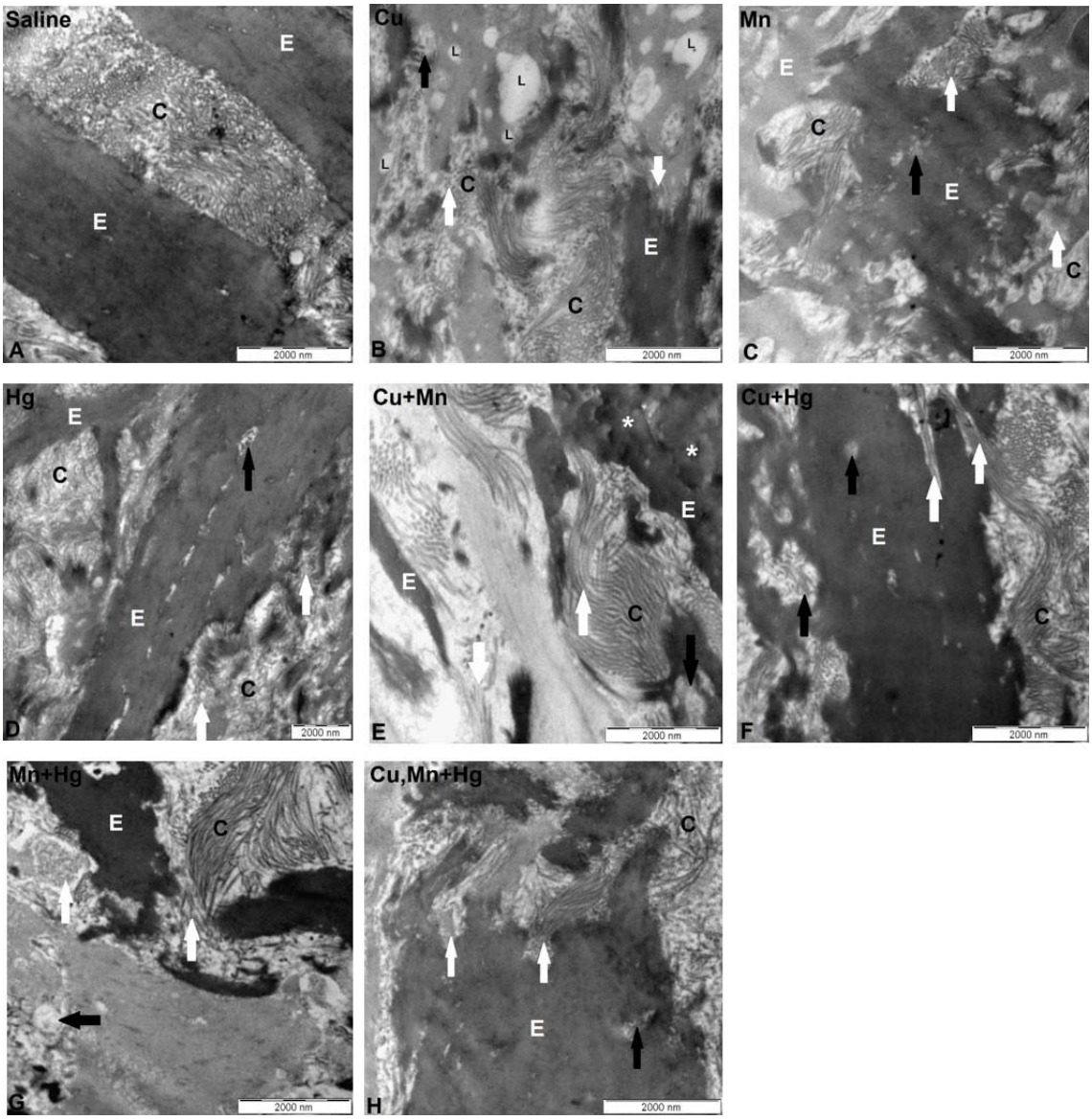

Figure 9: TEM micrographs of aortic tissue of SD rats exposed to Cu, Mn and Hg metal mixtures showing the ultrastructure of the tissue and demonstrating the arrangement of the collagen **(C)** and elastin **(E)** bands; Scale bar = 2 µm. **A**: Control, **B**: Cu, **C**: Mn, **D**: Hg, **E**: Cu + Mn, **F**: Cu + Hg, **G**: Mn + Hg, and **H**: Cu, Mn + Hg. **Black arrows**: Collagen deposition within elastin bands; **White arrows**: Collagen deposition instead of elastin; **White asterisk**: Elastin fragmentation and **L**: Lipids.

Aorta

Transmission electron microscopy

Representative aortic micrographs, acquired from control and exposed SD rat aortic tissue, are shown in Figure 9. In Figure 9 A, alternating bands of collagen (C) and

elastin (E) can be seen for the control (saline) group. The aortic collagen and elastin band arrangement of the experimental groups are shown in Figures 9 B - H. Overall, varying degrees of collagen and elastin disarrangement, collagen deposition within elastin bands (black arrows), and elastin disruption (white arrows) were present in all the experimental groups. Elastin electron density changes (lighter vs. darker areas) were also present in some groups – B, C, E and G. The Cu + Mn (Figure 9 E) group also showed elastin fragmentation (white asterisk) and the Cu group lipids (L) (Figure 9 B) within the tissue.

A summary on the ultrastructural findings of the aorta tissues is presented in Table 6 together with an assessment of the extent of the changes.

Table 6: Summary of the ultrastructural changes to aorta tissue following metal exposure.

	Disarranged bands	Collagen deposition (within)	Elastin disruption	Altered elastin electron density	Elastin fragmentation	Lipid accumulation
Cu	++	+	++	+	-	++
Mn	++	++	++	+	-	-
Hg	++	+	++	-	-	-
Cu + Mn	+++	++	+++	+	-	-
Cu + Hg	+	+++	+	-	-	-
Mn + Hg	+++	+	+++	++	+++	-
Cu, Mn + Hg	+	+	++	-	-	-

–: no or minimal alterations; +: slight alteration; ++: moderate alteration; +++: severe alteration

Heart

Transmission electron microscopy

Representative cardiac micrographs, acquired from control and exposed SD rat cardiac tissue, are shown in Figures 10 and 11. In Figures 10 and 11A well-organised and distinct mitochondria (M) with typical tubular cristae, myofibrils (MF) with clear Z lines (black arrows) and, myofibroblast (FB) having central nuclear condensation are visible in the control group. The cardiac myofibril-, mitochondria- and myofibroblast organisation and ultrastructure of the experimental groups are shown in Figures 10 and 11 B - H. Overall, varying degrees of distortion of the mitochondrial and myofibrillar parallel bands, interruption of Z lines, myofibrillar destruction and changes in mitochondrial ultrastructure and cristae were observed in the experimental groups. In the Cu group (Figure 10 and 11 B), the Z lines (black arrows) are still clear but appear thicker and the MF differ in thickness and are not uniform throughout. The Mn group (Figure 10 and 11 C) had Z lines (black arrows) that appeared darker,

unorganised MF and FB with chromatin condensation on the edges, closer to the membrane of the nucleus (N).

In the Hg group (Figure 10 and 11 D), the myofibrillar arrangement is disorganized, but the bands are still distinct with visible Z lines (black arrows) that are becoming less clear. In the Cu + Mn group (Figure 10 and 11 E), there are no clear myofibrillar bands or Z lines (black arrows) and the MF have been damaged evident by the presence of necrosis (black double asterisk) and mitochondrial replacement. The Cu + Hg group (Figure 10 and 11 F) showed large areas of MF being replaced with M and the myofibrils appeared less intact with blurred Z lines (black arrows) that are darker. In the Mn + Hg group (Figure 10 and 11 G), the M and the MF bands are distinct from each other with well-defined Z lines in the MF (black arrows). However, the MF appear to be replaced by M in some areas. In the triple mixture group (Figure 10 and 11 H), the tissue appeared to have undergone the most damage compared with the other experimental groups. There is no clear distinction between parallel bands of MF and M, and the Z lines (black arrows) are similar to the Cu + Mn group, but occur less frequently, which could be an indication of MF being replaced by M. The tissue also appears to have undergone necrosis (black double asterisk). The mitochondrial cristae appeared swollen in all experimental groups with the Cu + Mn (Figure 10 and 11 E) and Cu + Hg (Figure 10 and 11 F) groups having the most prominent changes as evident by the indistinct cristae. The Mn + Hg group (Figure 10 and 11 G) showed evidence of mitochondria vacuolation (black asterisk) and chromatin condensation appeared to be concentrated on the edges rather than the center of the nucleus (N).

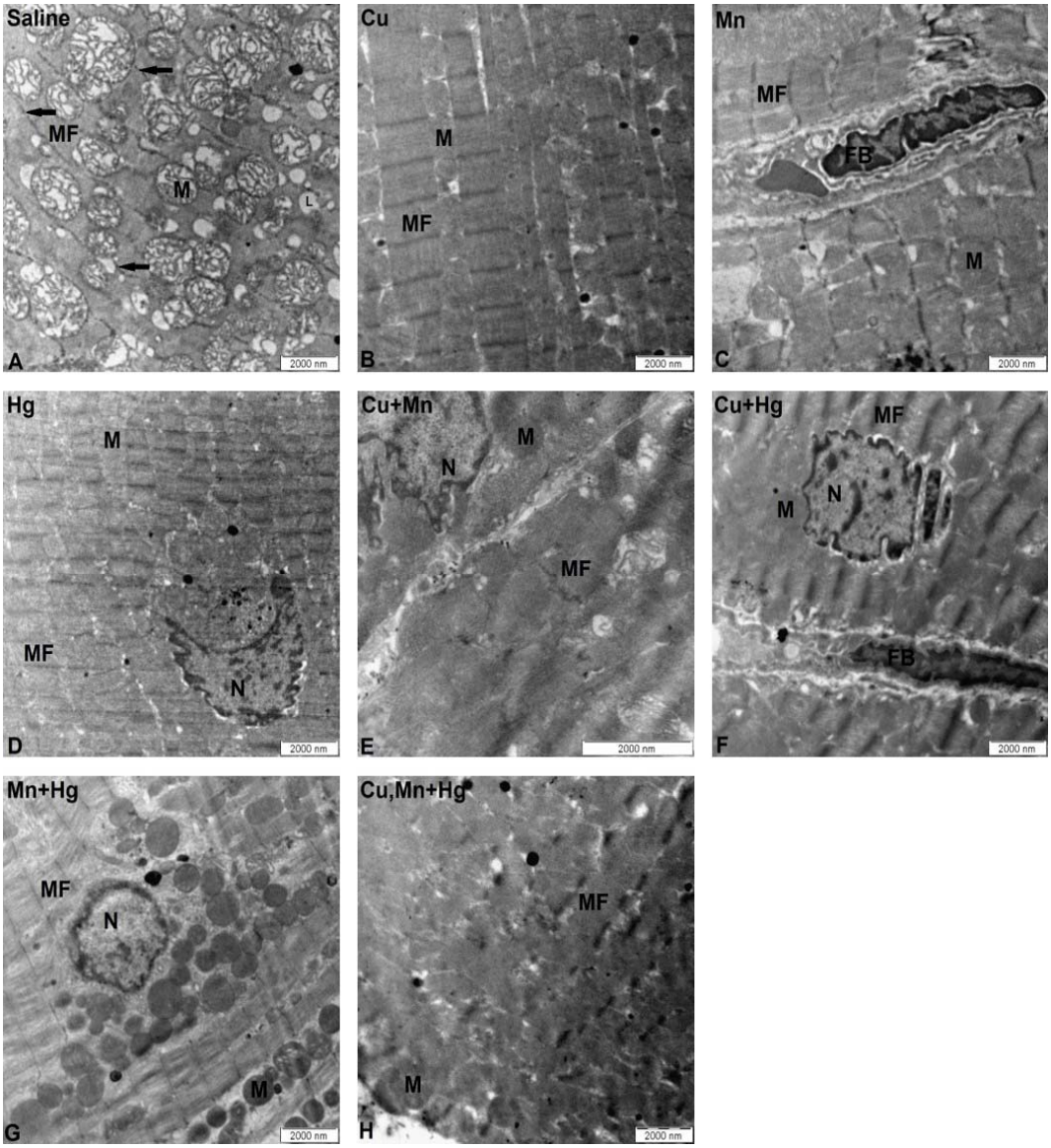

Figure 10: TEM micrographs of cardiac tissue of SD rats exposed to Cu, Mn and Hg metal mixtures showing the ultrastructure of the tissue and demonstrating the arrangement of the myofibrils and mitochondria at a lower magnification; Scale bar = 2 µm. **A**: Control, **B**: Cu, **C**: Mn, **D**: Hg, **E**: Cu + Mn, **F**: Cu + Hg, **G**: Mn + Hg, and **H**: Cu, Mn + Hg. **Black arrows**: Z line; **FB**: Fibroblast; **MF**: Myofibril; **M**: Mitochondria and **N**: Nucleus.

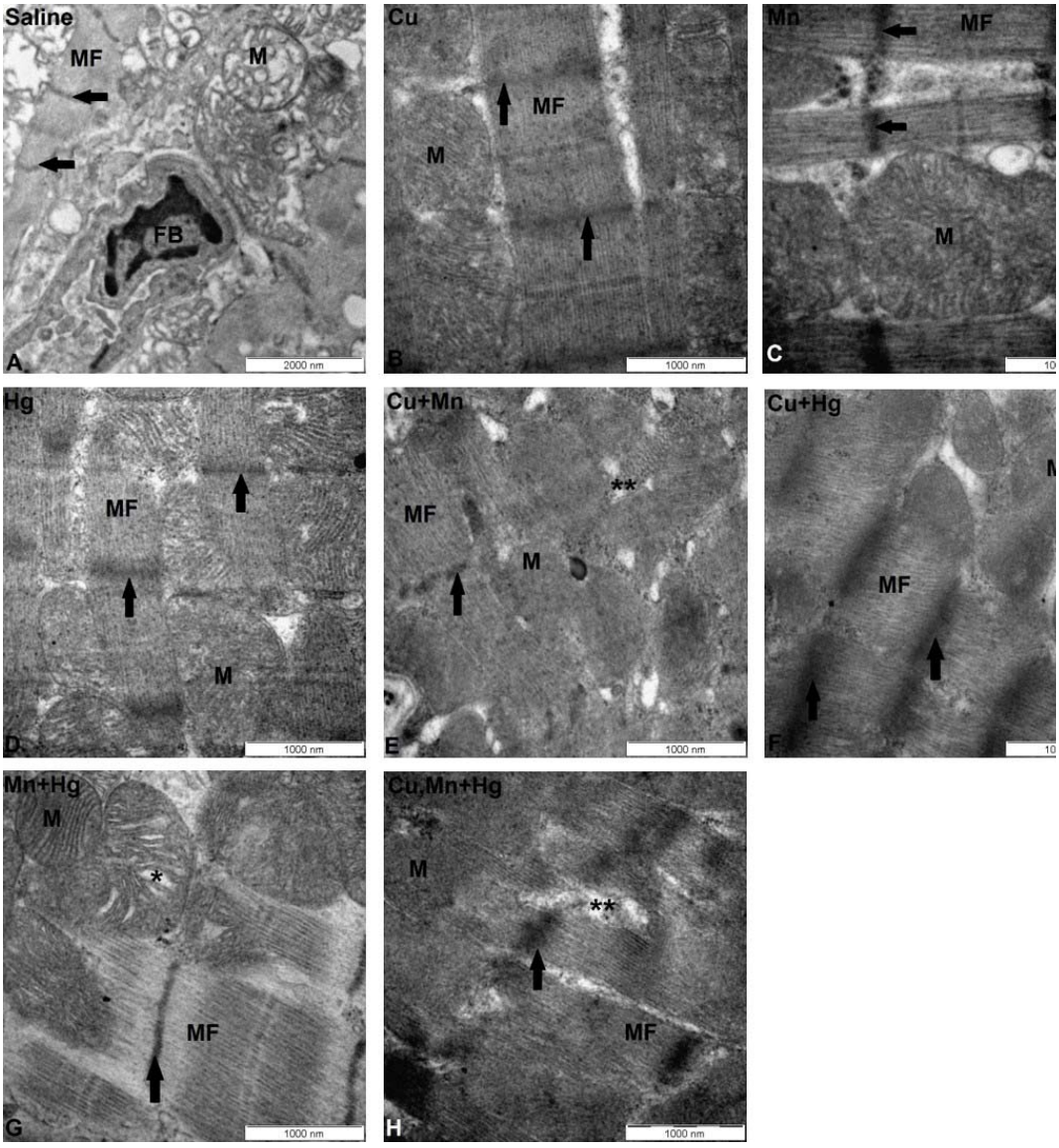

Figure 11: TEM micrographs of cardiac tissue of SD rats exposed to Cu, Mn and Hg metal mixtures showing the ultrastructure of the tissue and demonstrating the arrangement of the myofibrils and mitochondria at a higher magnification; Scale bar = 2 µm. **A**: Control, **B**: Cu, **C**: Mn, **D**: Hg, **E**: Cu + Mn, **F**: Cu + Hg, **G**: Mn + Hg, and **H**: Cu, Mn + Hg. **Black arrows**: Z line; **FB**: Fibroblast; **MF**: Myofibril; **M**: Mitochondria; **Black asterisk**: mitochondrial vacuolation and **Black double asterisk**: Necrosis.

A summary on the ultrastructural findings of the cardiac tissues is presented in Table 7 together with an assessment of the extent of the changes observed in the experimental groups.

Table 7: Summary of the ultrastructural changes to cardiac tissue following metal exposure.

	Disorganisation	Cristae swelling	Z line alterations	(M) vacuolation	Necrosis
Cu	+	++	+	-	-
Mn	+	++	+	-	-
Hg	++	++	++	-	-
Cu + Mn	+++	+++	+++	-	-
Cu + Hg	+++	+++	++	-	+
Mn + Hg	++	++	-	++	-
Cu, Mn + Hg	+++	+++	+++	-	++

–: no or minimal alterations; +: slight alteration; ++: moderate alteration; +++: severe alteration

Discussion

Blood parameters

Central to disease development are changes in blood haemostasis associated with inflammation and oxidative stress, which results in thrombosis through a combination of hypercoagulability, a disturbance in blood flow and endothelial damage (Roshan et al., 2011; Litvinov and Weisel, 2017; Grandl and Wolfrum, 2018). Previously we reported that Cu, Mn and Hg, alone and as part of mixtures, altered rat erythrocyte morphology, platelet activation as well as fibrin network formation associated with an increased risk of thrombosis (van Rensburg et al., 2020). In the present study, changes in the blood parameters were also evaluated. The measured parameters for RBCs in the control rats were slightly higher to that measured by He et al., 2017 for 250 male Sprague Dawley rats with a weight of 299.06 ± 22.6 g (He et al., 2017). Likewise the WCC, SNEU, LYM and PLT were slightly higher while the MON, EOS and BAS levels were within range.

Some RBC associated parameters were altered that may indicate some effects although the biological relevance may be limited. The numbers of each white blood cell type and platelets was unaltered. In general exposure via oral gavage to Cu, Mn and Hg alone and as part of mixtures caused minor changes to the blood parameters.

Aorta

Cardiovascular disease is a great threat to human health, globally (Cosselman et al., 2015). Type I atherosclerosis is described by the presence of isolated foam cells and macrophages forming an initial lesion (Stary et al., 1992; Stary, 2000; Komutrattanannont et al., 2018). Foam cells form when lipid droplet accumulation occurs within macrophages. Isolated foam cells are found in the TI layer, whereas macrophages without lipid droplet inclusions are found closer to the lumen (Stary et al., 1992). In the current study, isolated foam cells were present in the TI layer of all the experimental groups except for Cu + Hg (Figure 1), indicating the presence of early atherosclerosis. In this study, however, a thicker tunica media was only demonstrated in Mn, Cu + Hg and predominantly in Cu. Foam cells were present in all experimental groups, except Cu + Hg.

Ahmadi et al., (2017) found that rats fed an atherogenic diet had increased cholesterol levels and an irregular TI layer in the aorta (Ahmadi et al., 2017). Aortic histological studies further showed the presence of plaque (indicated by foam cells), fat deposits or vacuolation within the TM and the presence of dense irregular SMCN (Ahmadi et al., 2017). Elastic fibre structure was also altered as indicated by a wavy, interrupted arrangement. These alterations are associated with atherosclerosis (Ahmadi et al., 2017). An increase in the thickness of the TI and TM leading to aortic wall thickening is associated with aging and consequently decreased elasticity of the aorta (Komutrattanannont et al., 2018) leading to CVD. In hypertensive individuals, stiffness of the aorta is increased regardless of wall thickening (Liu et al., 2009). Saleh et al., (2017) and Thent et al., (2012) found that rats fed a high fructose diet, simulated a diabetic state. In these diabetic SD rats an increase in the thickness of the tunica media was found (Saleh et al., 2017). In the current study, the tunica media appeared thicker in the Cu, Mn and Cu + Mn groups (Figure 1 B, C and F) and this can indicate initial atherosclerotic changes.

The nuclei in most cells are oval or round and alterations in nuclear shape can be an indicator of disease or aging (Webster et al., 2009). Alterations in nuclear shape and thus rigidity will negatively affect tissues under mechanical stress (Webster et al., 2009). Changes in the shape of the nuclei and the uneven thickness of the aorta tissue are evident in all experimental groups. Changes in nuclear shape, tissue thickness

and perinuclear spaces were similarly seen in Cd, Hg and Cd + Hg exposed groups at X1000 the WHO safety limit (Arbi et al., 2021). The changes in the SMCN shape in the aorta tissue of the current study can thus be an indicator of loss of nuclear rigidity.

Exposure of aortic rings to Cu (1 hr at 10 µg/mL) decreases their contractile response due to an increase in reactive oxygen species (ROS) and in turn super oxide dismutase (SOD) activity resulting in elevated hydrogen peroxide (H_2O_2) and nitric oxide (NO) levels (Nunes et al., 2018). A decrease in contractibility may be due to a decrease in elastin and thus the loss of integrity of the aortic tissue, which may result in aneurysms (Chung et al., 2007). In the current study, the Cu group had the severest increase in the tunica media thickness, which could be an indicator of dilation and thus increasing the risk of the future rupture of the aorta or aortic aneurysm as Völker et al., (1997) suggested. Völker et al., (1997) also found an accumulation of SMC, macrophages, foam cells, leucocytes and ECM formation, leading to a fibrotic thickening and narrowing of the lumen to occur (Völker et al., 1997) substantiating the findings of this study as well although the ionic concentration is not identical to this study.

Manganese inhibits Ca^{2+} from entering SMCs, which alters contractility and in turn vascular diameter (Nasu et al., 1995; Ettarh, 2004; Amberg and Navedo, 2013). A decrease in intracellular Ca^{2+} concentration causes a decrease in SMC contractility and results in vasodilation and consequently hypotension, an effect observed with Mn (Jiang and Zheng, 2005; Amberg and Navedo, 2013). In the current study, the Mn group increased the abundance of connective tissue (collagen). Mercury has many toxic effects on the vascular system, including increasing the thickness of the intimal- and medial layers, causing atherosclerosis (Houston, 2011). Mercury causes vasodilation by producing NO and is a Ca^{2+} channel agonist due to ROS production. Nitric Oxide causes the phosphorylation and thus activation of the potassium ion (K^+) ATP channel (Omanwar et al., 2014). In the current study, the Hg concentration was not high enough to cause the same alterations as what was observed with Mn and thus can be presumed that Hg does not alter Ca^{2+} levels to the same extent as Mn.

The TA predominantly consists of collagen and elastin fibres as well as fibroblasts (Gallicchio, 2001) and was thought to only provide physical support and nutrition to the blood vessel wall, but has been identified as a highly cellular- and metabolically

active layer that can alter the structure, function and progression of disease of the blood vessel walls (Ogeng'o et al., 2014). Atherogenic changes to the TA can take place before changes to the TI or TM layers occur (Ogeng'o et al., 2014). In the current study, several groups showed an increase in yellow-red birefringence, associated with an increase in collagen type I accumulation. The extent of accumulation ranked in descending order from Mn + Hg> Cu + Mn> Mn> Cu. Collagen type I and III are the most common collagen types present in the arterial wall, with type I being associated with providing arterial stiffness and type III providing arterial dilatability. Thus, an increase in collagen type I will cause an increase in arterial stiffness, which will increase aortic fibrosis and can contribute to the development of aortic dissection or aneurysm (Wang et al., 2006).

On the ultrastructural level, overall, all the experimental groups exhibited adverse effects on aortic tissue. The group with the most prominent changes is the Mn + Hg group, but interestingly with added Cu, this group resembles more closely the control group. The triple mixture group demonstrated no or slight alterations for most of the features identified. This clearly demonstrates how different metal mixtures can either have synergistic (Mn + Hg), additive or antagonistic (Cu, Mn + Hg) effects on each other.

The ultrastructural changes in quantity or architecture of collagen and elastin fibres causes changes to the mechanical (elasticity and tensile strength) and thus functional properties of aortic tissue, resulting in disease. In the current study, the experimental groups showed disarrangement of collagen and elastin bands and the deposition of collagen within elastin or elastin disruption. The Mn + Hg group (Figure 9 G) was the only group that demonstrated elastin fragmentation, whereas the Cu only group (Figure 9 B) demonstrated the presence of lipids. An aging aorta is characterised by a decrease in elastin because of an increase in the quantity of collagen (from 20% to a range of 26% to 31%). Disarrangement of collagen fibres in the TM and cross-linking of collagen fibres also occur during ageing. Fragmentation of elastin also occurs during ageing possibly because of mechanical failure or through chemical degradation by matrix metalloproteinases (MMP's). An increase in expression of MMP's is also associated with calcification of aortas (Tsamis et al., 2013). Thus, the Mn + Hg group qualitatively appeared to have the highest degree of inflammation in the aorta due to

the presence of fragmented elastin hypothesised to be the result of increased MMP's (Tsamis et al.,, 2013; Shoulders and Raines, 2009; van Doren, 2015).

Heart

Cardiomyopathies may lead to electrical or mechanical dysfunction and are characterized by myocardial dilatation, hypertrophy, and restrictive pathologies that can all result in heart failure (Machackova et al., 2006; Schultheiss et al., 2019). The aetiology of cardiomyopathies can be genetic or acquired (Machackova et al., 2006). In the current study, the experimental groups demonstrated some features associated with the inherited dilation or hypertrophic cardiomyopathies. Tissue dilation was present in all the experimental groups with the Cu + Hg and the triple mixture groups demonstrating a moderate alteration. All the experimental groups also demonstrated an increase in ECM and cardiomyocyte disarray with the Mn, Cu + Mn and Cu + Hg groups having a moderate increase in ECM.

Some metals are known to cause toxic cardiomyopathies. Cobalt causes reduced ATP production and contractile dysfunction; antimony causes lethal oxidative stress and apoptosis due to increased intracellular Ca^{2+} and Hg causes a reduction in GSH, increased ROS production and disruption of enzymatic reactions dependant on selenium (Hantson, 2019). In the current study, all the experimental groups demonstrated some degree of cardiomyocyte disarray and loose myofibrillar arrangement, resulting in tissue dilation. Along with these features, myofibril destruction was severe in the Cu + Mn and Cu + Hg groups, moderate in Mn, Mn + Hg and the triple mixture groups and the least in the Cu and Hg groups. Interestingly, the severely damaged myocytes were accompanied with lymphocyte infiltration, indicating inflammation. The triple mixture group was the only group where lymphocyte infiltration occurred without severe myocytes destruction. Inflammation occurs due to myocardial tissue damage and is associated with myocardial infarction. This process is initiated to repair damaged tissues, which have undergone cellular necrosis because of a lack of oxygen. This allows healing, remodelling of the tissue and scar formation (Hofmann and Frantz, 2015). The current study does clearly depict a degree of dilatation in the cardiac tissue. Although myocyte disarray, as seen in the current study, is a hallmark feature in myocardial hypertrophy, it is possible for dilatation and

hypertrophy of cardiac tissue to occur simultaneously (Garcia-Canadilla et al., 2019; Nahrendorf et al., 2005).

All experimental groups show some degree of ECM deposition with Mn, Cu + Mn and Cu + Hg demonstrating the greatest increase amongst all the groups, when stained with H&E. After PR staining, Cu + Hg demonstrated a severe increase and Mn a slight increase in collagen type I around blood vessels. Type I collagen was also moderately increased in Cu + Hg and type III collagen was slightly increased in Mn, within the myocardium. The lack of birefringence in the Cu + Mn group may be an indicator of an increase in other ECM proteins or molecules other than collagen type I and III. The triple mixture group showed the greatest increase in type III collagen, both around the blood vessels and within the myocardium. Type III collagen is predominantly found in the endomysium and the expansion of the endomysium (increase in type III collagen in other areas as demonstrated in the triple mixture group), is associated with interstitial fibrosis (Frangogiannis, 2019).

Physiologically, lipid accumulation occurs predominantly in adipocytes and minimally in the liver and muscle tissues (Schulze, 2009; Marfella et al., 2009). Lipid accumulation within the myocardium occurs during heart failure. Individuals with metabolic syndrome or associated conditions such as diabetes, obesity and hypertension, are at a higher risk of cardiac disease and heart failure (Schulze, 2009). In the current study, a slight increase in lipid accumulation occurred in the Cu, Hg, Cu + Hg and Cu, Mn + Hg groups and moderately in the Mn group. Interestingly, when Mn was combined with Cu or Hg no increase in lipid droplets was observed. This may suggest antagonistic effects of Cu and Hg on Mn. In contrast, the effects of Cu and Hg are synergistic or additive. The amount of lipid accumulation seen in the current study is far less compared with lipid accumulation in failing heart biopsies of individuals with metabolic syndrome (Marfella et al., 2009).

Arbi et al., (2021) found similar effects for Cd, Hg and co-exposed rats at X1000 the WHO water safety limits. The authors found the irregular, loose appearance of myofibrils, deformation of the shape of the nuclei, and myofibril disarray in all experimental groups. The Hg group demonstrated myofibril destruction and the formation of vacuoles (Arbi et al., 2021). Karaboduk et al., (2015) reported multiple toxic effects in male Wistar rats administered $HgCl_2$ at 1.0 mg/kg. These effects

included inflammatory cell infiltration, disorganisation of myofibrils, myocyte degeneration, tissue oedema and necrosis (Karaboduk et al., 2015). A study done by Baiyun et al., (2018) demonstrated cardiotoxicity in Wistar rats administered 80 mg/L of $HgCl_2$. On ultrastructural level, the characteristic parallel bands of myofibrils and mitochondria became disorganised following metal exposure in the current study. Swelling of mitochondrial cristae was also evident in all mixtures of metals. Alterations in Z lines were evident in all metal mixtures, except for the Mn + Hg group. However, interestingly the Mn + Hg group was the only group to exhibit mitochondrial vacuolation. Necrosis only occurred in the triple mixture group and in Cu + Hg.

Apoptosis, necrosis and autophagy leads to cellular death via varying pathways. Common morphological features of these three cellular death modalities, is nuclear fragmentation and mitochondrial damage. There is cross-talk between all three modalities depending on the type of stimulus the toxicant exhibits for example an increase in ROS, decrease in ATP or damage to a particular organelle. Autophagy has been observed in many biopsies of patients that had CVD. The inhibition of autophagy results in a reduced number of cardiomyocytes that are able to survive under stress (Orrenius et.al., 2012). The disorganisation, alterations in Z lines and cristae swelling demonstrated in all the experimental groups, negatively impacts on cardiomyocyte function and consequently the contractibility of the heart. However, these damaging features are reversible if toxic exposure ceases. The triple mixture group, showed the most cardiac toxicity and although the Mn + Hg group did not show necrosis of myofibrils, it did exhibit mitochondrial necrosis through vacuolation.

Conclusion

In conclusion, the rats exposed to Cu, Mn and Hg, alone or as part of mixtures, had an increase in plasma metal levels and some changes although minor changes in the measured FBC parameters. All the heavy metal groups demonstrated toxic effects on tissue morphology and ultrastructure. The tissues differed in sensitivity to the various metals and their mixtures. The Cu group demonstrated a TM that appeared substantially thickened. The Mn group caused drastic connective tissue deposition and Hg had the most altered morphological features. The Cu + Mn and Mn + Hg groups had the most severe feature changes including an increase in collagen type I. The Cu + Hg group also had the most morphological changes, with the most severe being in

the heart tissue. The aorta was most sensitive to the Mn + Hg mixture, which demonstrated an increase in collagen deposition, elastin density, elastin fragmentation and the disarrangement of these fibres. The Cu + Mn and triple mixture groups caused severe alterations to both myofibrils and mitochondria. However, the Mn + Hg mixture was the only group that exhibited the necrotic feature of mitochondrial vacuolation. These results indicate some cellular dysfunction possibly related to oxidative stress.

References

Ahmadi K, Wulansari A, Yunianta Y, Estiasih Teti (2017). Protective effect of food products enriched with unsaponifiable matter from palm fatty acid distillate on the aorta of hypercholesterolemic rats. Journal of Applied Pharmaceutical Science 7(12): 90-96.

Alissa EM, Ferns GA (2011). Heavy metal poisoning and cardiovascular disease. Journal of Toxicology 870125

Amberg GC, Navedo MF (2013). Calcium dynamics in vascular smooth muscle. Microcirculation 20(4): 281-289.

Angelova M, Asenova S, Nedkova V (2011). Copper in the human organism. Trakia Journal of Sciences 9(1): 88-98.

Arbi S, Bester MJ, Pretorius L, Oberholzer HM (2021). Adverse cardiovascular effects of exposure to cadmium and mercury alone and in combination on the cardiac tissue and aorta of Sprague-Dawley rats. Journal of Environmental Science *and* Health, Part A: Toxic/Hazardous Substances *and* Environmental Engineering 56(6): 609-624.

Baiyun R, Li S, Liu B, Lu J, Lv Y, Xu J, Wu J, Li J, Lv Z, Zhang Z (2018). Luteolin-mediated PI3K/AKT/Nrf2 signaling pathway ameliorates inorganic mercury-induced cardiac injury. Ecotoxicology and Environmental Safety 161: 655-661.

Chung AW, Au Yeung K, Sandor GG, Judge DP, Dietz HC, van Breemen C (2007). Loss of elastic fibre integrity and reduction of vascular smooth muscle contraction resulting from the upregulated activities of matrix metalloproteinase-2 and -9 in the thoracic aortic aneurysm in Marfan syndrome. Circulation Research 101(5): 512-522.

Cosselman KE, Navas-Acien A, Kaufman JD (2015). Environmental factors in cardiovascular disease. Nature Reviews Cardiology 12(11): 627-642.

Crossgrove J, Zheng W (2004). Manganese toxicity upon overexposure. Nuclear Magnetic Resonance in Biomedicine 17(8): 544-553.

Ettarh RR (2004). Inhibitory effect of manganese on contraction of isolated rat aorta. Indian Journal of Experimental Biology 42(2): 149-151.

Ferkol T, Schraufnagel D (2014). The global burden of respiratory disease. Annals of the American Thoracic Society 11(3): 404-406.

Frangogiannis NG (2019). Cardiac fibrosis: Cell biological mechanisms, molecular pathways and therapeutic opportunities. Molecular Aspects of Medicine 65: 70-99.

Gallicchio MA (2001) Culture of human smooth muscle cells. Methods in Molecular Medicine 52: 137-146.

Garcia-Canadilla P, Cook AC, Mohun TJ, Oji O, Schlossarek S, Carrier L, McKenna WJ, Moon JC, Captur G (2019) Myoarchitectural disarray of hypertrophic cardiomyopathy begins pre-birth. Journal of Anatomy 235(5): 962-976.

Grandl G. Wolfrum C (2018) Hemostasis, endothelial stress, inflammation, and the metabolic syndrome. Seminars in Immunopathology. Springer, pg 215-224.

Hantson P (2019) Mechanisms of toxic cardiomyopathy. Clinical Toxicology 57(1): 1-9.

He Q, Su G, Liu K, Zhangm F, Jiang Y, Gao J, Liu L, Jiang Z, Jin M, Xie H (2017) Sex-specific reference intervals of hematologic and biochemical analytes in Sprague-Dawley rats using the nonparametric rank percentile method. PLoS One 12(12): e0189837.

Hofmann U, Frantz S (2015) Role of lymphocytes in myocardial injury, healing, and remodelling after myocardial infarction. Circulation Research 116(2): 354-367.

Houston MC (2011) Role of mercury toxicity in hypertension, cardiovascular disease and stroke. Wiley Periodicals 13: 621-627

Hunt C (2009) Proceedings of the VIIIth Conference of the International Society for Trace Element Research in Humans (ISTERH), the IXth Conference of the Nordic Trace Element Society (NTES), and the VIth Conference of the Hellenic Trace Element Society (HTES), 2007. Springer: pg 5-7.

Jaishankar M, Tseten T, Anbalagan N, Mathew BB, Beeregowda KN (2014) Toxicity, mechanism and health effects of some heavy metals. Interdisciplinary Toxicology 7(2): 60-72.

Jiang Y, Zheng W (2005) Cardiovascular toxicities upon manganese exposure. Cardiovascular Toxicology 5(4): 345-354.

Jomova K, Valko M (2011) Advances in metal-induced oxidative stress and human disease. Toxicology 283(2 – 3): 65-87.

Kampa M, Castanas E (2008) Human health effects of air pollution. Environmental Pollution 151(2): 362-367.

Karaboduk H, Uzunhisarcikli M, Kalender Y (2015) Protective effects of sodium selenite and vitamin e on mercuric chloride-induced cardiotoxicity in male rats. Brazilian Archives of Biology and Technology 58(2): 229-238

Kierszenbaum AL, Tres L (2016) Histology and Cell biology: An Introduction to Pathology. 4th Ed. Elsevier Saunders.

Kim D, Chen Z, Zhou LF, Huang SX (2018) Air pollutants and early origins of respiratory diseases. Chronic Diseases and Translational Medicine 4(2): 75-94.

Komutrattananont P, Mahakkanukrauh P, Das S (2019) Morphology of the human aorta and age-related changes: anatomical facts. Anatomy Cell Biology 52(2): 109-114.

Kumar SV, Bhattacharya S (2000) In vitro toxicity of mercury, cadmium and arsenic to platelet aggregation: influence of adenylate cyclase and phosphodiesterase activity. In Vitro and Molecular Toxicology 13(2): 137-144.

Lattouf R, Younes R, Lutomski D, Naaman N, Godeau G, Senni K, Changotade S (2014) Picrosirius red staining: a useful tool to appraise collagen networks in normal and pathological tissues. Journal of Histochemical Cytochemistry 2(10): 751-758.

Lim KM, Kim S, Noh JY, Kim K, Jang WH, Bae ON, Chung SM, Chung JH (2010) Low-level mercury can enhance procoagulant activity of erythrocytes: A new contributing factor for mercury-related thrombotic disease. Environmental Health Perspectives 118(7): 928-935.

Litvinov RI, Weisel JW (2017) Role of red blood cells in haemostasis and thrombosis. International Society of Blood Transfusion: Science Series 12(1): 176-183.

Liu X, Pu F, Fan Y, Deng X, Li D, Li S (2009) A numerical study on the flow of blood and the transport of LDL in the human aorta: the physiological significance of the helical flow in the aortic arch. American Journal of Physiology- Heart and Circulatory Physiology 297(1): 163-170.

Machackova J, Barta J, Dhalla NS (2006) Myofibrillar remodelling in cardiac hypertrophy, heart failure and cardiomyopathies. Canadian Journal of Cardiology 22(11): 953-68.

Marfella R, Di Filippo C, Portoghese M, Barbieri M, Ferraraccio F, Siniscalchi M, Cacciapuoti F, Rossi F, D'Amico M, Paolisso G (2009) Myocardial lipid accumulation in patients with pressure-overloaded heart and metabolic syndrome. Journal of Lipid Research 50: 2314-2323.

Mudgal V, Madaan N, Mudgal A, Singh RB, Mishra S (2010) Effect of toxic metals on human health. The Open Nutraceuticals Journal 3: 94-99.

Nahrendorf M, Spindler M, Hu K, Bauer L, Ritter O, Nordbeck P, Quaschning T, Hiller KH, Wallis J, Ertl G, Bauer WR, Neubauer S (2005) Creatine kinase knockout mice show left ventricular hypertrophy and dilatation, but unaltered remodelling post-myocardial infarction. Cardiovascular Research 65(2): 419-427.

Naidoo SVK, Bester MJ, Arbi S, Venter C, Dhanraj P, Oberholzer HM (2019) Oral exposure to cadmium and mercury alone and in combination causes damage to the

lung tissue of Sprague-Dawley rats. Environmental Toxicolology and Pharmacology 69: 86-94.

Nair AB, Jacob S (2016) A simple practice guide for dose conversion between animals and human. Journal of Basic and Clinical Pharmacy 7(2): 27-31.

Nasu T, Murase H, Shibata H (1995) Manganese ions penetrate via L-type Ca^{2+} channels and induce contraction in high-K^{+} medium in ileal longitudinal muscle of guinea-pig. General Pharmacology 26(2): 381-386.

Nunes KZ, Fioresi M, Marques VB, Vassallo DV (2018) Acute copper overload induces vascular dysfunction in aortic rings due to endothelial oxidative stress and increased nitric oxide production. Journal of Toxicology and Environmental Health, Part A 81(8): 218-228.

Ogeng'o J, Ongeti K, Obimbo M, Olabu B, Mwachaka P (2014) Features of atherosclerosis in the tunica adventitia of coronary and carotid arteries in a black kenyan population. Anatomy Research International 1-5.

Olowoyo JO, Okedeyi OO, Mkolo NM, Lion GN, Mdakane STR (2012) Uptake and translocation of heavy metals by medicinal plants growing around a waste dump site in Pretoria, South Africa. South African Journal of Botany 78: 116-121.

Omanwar S, Saidullah B, Ravi K, Fahim M (2014) Vasorelaxant effects of mercury on rat thoracic aorta: the nitric oxide signalling mechanism. Human Experimental Toxicology 33(9): 904-910.

O'Neal SL, Lee JW, Zheng W, Cannon JR (2014) Subacute manganese exposure in rats is a neurochemical model of early manganese toxicity. Neurotoxicology: 44 303–313.

Orrenius S, Kaminskyy VO, Zhivotovsky B (2012) Autophagy in toxicology: cause or consequence? Annual Review of Pharmacology and Toxicology 53: 275-297.

Roshan VD, Assali M, Moghaddam AH, Hosseinzadeh M, Myers J (2011) Exercise training and antioxidants: effects on rat heart tissue exposed to lead acetate. International Journal of Toxiciology 30(2): 190-196.

Saleh R, Merghani BH, Awadin W (2017) Effect of high fructose administration on histopathology of kidney, heart and aorta of rats. Journal of Advanced Veterinary and Animal Research 4(1): 71-79.

Schultheiss HP, Fairweather D, Caforio ALP, Escher F, Hershberger RE, Lipshultz SE, Liu PP, Matsumori A, Mazzanti A, McMurray J, Priori SG (2019) Dilated cardiomyopathy. Nature Reviews Disease Primers 5(1): 32-108.

Sengupta P (2013) The laboratory rat: Relating its age with human's. International Journal of Preventive Medicine 4(6): 624-630.

Shoulders MD, Raines RT (2009) Collagen structure and stability. Annual Review of Biochemistry 78: 929-958.

Shulze PC (2009) Myocardial lipid accumulation and lipotoxicity in heart failure. Journal of Lipid Research 50(11) 2137-2138.

Stary HC, Blankenhorn DH, Chandler AB, Glagov S, Insull WJ, Richardson M, Rosenfeld ME, Schaffer SA, Schwartz CJ, Wagner WD, Wissler RW (1992) A definition of the intima of human arteries and of its atherosclerosis-prone regions. Circulation 85: 391-405.

Stary HC (2000) Lipid and macrophage accumulations in arteries of children and the development of atherosclerosis. The American Journal of Clinical Nutrition 72(5 Suppl) 1297S-1306S.

Thent ZC, Lin TS, Das S, Zakaria Z (2012) Histological changes in the heart and the proximal aorta in experimental diabetic rats fed with Piper sarmentsoum. African Journal of Traditional Complement Alternative Medicine 9(3): 396-404.

Tsai NC, Lee RM (2011) Interaction between cardiovascular system and respiration. Applied Mathematical Modelling 35(11): 5460–5469.

Tsamis A, Krawiec JT, Vorp DA (2013) Elastin and collagen fibre microstructure of the human aorta in ageing and disease: a review. Journal of the Royal Society Interface 10(83): 1-22.

van Doren SR (2015) Matrix metalloproteinase interactions with collagen and elastin. Matrix Biology. Journal of the International Society for Matrix Biology 44-46: 224–231

van Rensburg MJ, van Rooy MJ, Bester MJ, Serem JC, Venter C, Oberholzer HM (2019) Oxidative and haemostatic effects of copper, manganese and mercury, alone and in combination at physiologically relevant levels: An ex vivo study. Human and Experimental Toxicology 38: 419-433.

Velindala S, Gaikwad P, Ella KKR, Bhorgonde KD, Hunsingi P, Anop K (2014) Histochemical analysis of polarizing colours of collagen using Picro Sirius red staining in oral submucous fibrosis. Journal of Oral Health 6(1): 33-38.

Venter C, Oberholzer HM, Bester J, Van Rooy MJ, Bester MJ (2017) Ultrastructural, confocal and viscoelastic characteristics of whole blood and plasma after exposure to cadmium and chromium alone and in combination: An ex vivo study. Cellular Physiology and Biochemistry 43: 1288-1300.

Völker W, Dorszewski A, Unruh V, Robenek H, Breithardt G, Buddecke E (1997) Copper-induced inflammatory reactions of rat carotid arteries mimic restenosis/arteriosclerosis-like neointima formation. Atherosclerosis 130(1-2): 29-36.

Wang X, LeMaire SA, Chen L, Shen YH, Gan Y, Bartsch H, Carter SA, Utama B, Ou H, Coselli JS, Wang XL (2006) Increased collagen deposition and elevated expression of connective tissue growth factor in human thoracic aortic dissection. Circulation 114(1): 200-205.

Webster M, Witkin KL, Cohen-Fix O (2009) Sizing up the nucleus: nuclear shape, size and nuclear-envelope assembly. Journal Cell Science 122: 1477-86.

World Health Organisation. Guidelines for drinking-water quality: fourth edition (2011). [Internet]. [Cited May 2018]. Available from: https://www.unicef.org/ cholera/Chapter_4_prevention/01_WHO_ Guidelines_for_drinking_water_quality.pdf.